Bachelor Thesis
Element gradients in the Solar neighborhood affecting terrestrial planet composition

by, David M. Jorge s3315886
supervisor, Prof. Dr. I.E.E. Kamp
second reader, Prof. Dr. F.F.S. van der Tak

03 July 2020

Abstract

In the following research we investigate the influence of the equilibrium condensation sequence for various element mixtures using the computer code GGchem. We model a pressure-temperature radial disk profile and use the Hypatia catalog as database for the stellar abundances. We are studying the impact on planet composition when the ratios Fe/Mg, Mg/Si and Fe/S are changed from the Solar abundance values. The study is done using six different stars and the Sun as reference. We discover that using elements ratios typical of the spread shown in main sequence G-type stars in the Solar neighborhood leads in large changes in the type of condensates formed using GGchem. Moreover, the condensed phase from which the planets form does not reflect the initial elements ratios present in the gas phase. Ratios of refractory elements such as Mg/Si translate directly from the gas phase to the condensed phase if the planet form below T< 1000 K. However, ratios with respect to volatile elements such as oxygen change from one phase to the other. Our study show that to accuratly investigate the composition of planets, one needs to take into account the abundances of the stellar system under investigation, and study the condensation of the protoplanetary disk as the resulting condensed phase will have different abundance ratios.

1 Introduction

In the interstellar medium, molecular clouds give rise to the conditions necessary for stellar formation. Upon reaching its Jeans' Mass[1], the cloud fragments into collapsing clouds. Given the law of conservation of angular momentum, any initial rotational velocity that the cloud had will force it to rotate faster as it collapses upon itself, flattening the cloud at its poles, giving it its characteristic flat protoplanetary disk. The primordial composition of the disk is essentially made out of the same initial material that was contained in the collapsing cloud. Hydrogen, helium, as well as metals can be found in various degrees of abundance. The stellar object at its center heats the dust grains in the disk, it will do so more efficiently for those sitting nearest to its surface. As one observes the temperature within the disk, and along its radius in the mid plane (where planets form), one will find it decreasing. As the temperature drops, chemical elements binds together forming more complex molecules, and eventually change phase from gas to liquid/solid. These condensates, will in turn agglomerate forming a solid body increasing in size and mass, eventually reaching a point where it becomes a planet orbiting its host star.

Potentially, all chemical elements initially composing the protoplanetary disk will condensate and be part of the forming planets. The physical and chemical processes happening during this formation will be influenced by many factors, including the temperature, the pressure, and chemical composition of the protoplanetary disk during the condensation. In that regard, while pressure-temperature profile, as well as chemical processes are paramount in determining the final product of the condensation sequence, the various

[1]Minimal mass value in order for the gravity of the cloud to overcome the internal outward pressure of the gas.

chemical elements have very disparate influences on the final body. As a matter of fact, terrestrial planets are mainly composed of elements such as Mg, Si, Fe and O. The ratios of these different elements control various aspects of a planet such as the composition and relative sizes of the different structures of the body (upper/lower mantle, core size). Moreover, S is a very interesting chemical element when it comes to probe the identity of lighter elements present in the core. Therefore, it becomes important to know what kind of impact one would expect from varying the ratios of these elements from those found in our Sun.

These discrepancies from the Solar values can be attributed to processes such as Type Ia supernovae (Hinkel et al., 2014). Moreover, Kobayashi and Nakasato, 2011 show, using chemodynamical simulations of a Milky-Way-type galaxy that the ratio of certain elements with respect to Fe vary as well. The code that they used included not only supernova feedback, but chemical enrichment as well. Therefore, variation from the Solar norm of refractory elements is a well established fact. The question remaining to answer is to know whether, what has been considered by many as a small fluctuation in the ratio of the refractory elements (factor two or three difference), has a noticeable impact on the composition as well as the structure of a body condensing from a protoplanetary disk.

In the following paper, we will investigate the equilibrium condensation sequence for various element mixtures using a computer code available to us (GGchem). In particular, we will vary the abundances needed to run the algorithm (from Solar abundance) in accordance with observational data. We will study how these variations propagate into the chemical composition of disks that surround main sequence G-type stars and what impact these results have on planet formation. Researches in planet formation often assume that the elements ratios found in the gas phase directly translate in the condensed phase from which planets form. Our study stands out as we are trying to take a step back and see if this assumption holds up when stellar abundances are changed from the Solar abundance values.

For the purpose of planet building, it is important to know the abundance of the condensates composing the mass that will form the object. In order to accomplish that aim, we have taken three steps. First, in Section 2 we will discuss GGchem, as well as the protocol used to derived the condensation sequences of each element entering the primordial mixture of the protoplanetary disk. Secondly, in Section 3, we will investigate the variations in the ratio of the refractory elements Mg, Si and Fe found in the Solar neighborhood (within 150 pc of the Sun). Finally, in Section 4, we will explain and calculate the pressure-temperature profile used to model the cooling happening within the disk as one goes ever further from the central star.

To analyse these results we will take two different paths. In Section 5.1 and Section 5.2 we will look at the impact of the ratios of refractory elements on the condensation of Mg- and Fe-condensates, while in Section 5.3 we will look at the chemical composition of five hypothetical planets. Moreover, we will investigate how chemical ratios with respect to volatile elements such as oxygen change from the gas phase (in the protoplanetary disk before condensation) to the condensed phase (after the condensation of the protoplanetary disk).

2 The GGchem code

The code used in this paper is the GGchem code. It was first developed by Gail and Sedlmayr, 1986 and subsequently improved upon by C. Dominik, Ch. Helling and P. Woitke up until 2005. However, the version currently being used is a totally new version, re-written in a modern FORTRAN-90 code architecture (Woitke et al., 2018). The major improvement that this new version of the code offers, is the possibility to go down to a temperature of 100 K, thanks to the use of quadruple precision arithmetic. The various thermo-chemical data implemented in the GGchem code are taken from the NIST-JANAF database (Chase et al., 1982, Jr, 1986) and the geophysical SUPCRTBL database (Zimmer et al., 2016, Johnson et al., 1992). The GGchem code has been thoroughly benchmarked against the values found in the public thermo-chemical equilibrium abundances (TEA) code (Blecic et al., 2016) and has been found to agree remarkably well.

GGchem allows for the determination of the composition of gases in thermochemical equilibrium (forward and reverse reactions are happening at the same rate) by minimizing the Gibbs free energy G. This energy represents the chemical potential of an isothermal thermodynamical system. A value of $\Delta G > 0$ is indicator of a spontaneous process while $\Delta G < 0$ indicates non-spontaneous processes. As such, to minimise the

Gibbs free energy (e.g. $\Delta G = 0$) is to reach equilibrium between all potential components of the gas (atoms, molecules) for a given pressure and temperature. The code also allows the inclusion of equilibrium condensation, which leads the chemical species, under the right conditions, to condensate as liquids or solid in the gas. This in turn, produces a condensation sequence and is the base used for deriving the composition of a solid body condensing from a gas cloud.

A total of 24 elements (H, He, Li, C, N, O, Na, Mg, Al, Si, S, Cl, K, Ca, Ti, V, Cr, Mn, Fe, Ni, Zr, W, F, P), as well as charged species, can be selected as input. Furthermore, the initial abundance of each of these chemical elements must be specified. Depending on this initial choice, GGchem will form molecules and condensate species accordingly.

The O-dimensional analysis of GGchem is calculated given a temperature. The code can accordingly calculate the state of the system using the ideal gas law and derive the pressure at that temperature. However, a higher dimensional approach can be taken, where a specific pressure-temperature radial disk profile is input into GGchem (1-dimensional). A 2-dimensional approach could as well be used, where a range of temperatures and pressures are independently given to the code, which generates phase diagrams spanning the entire pT-plane. Regardless of the approach taken, given a specific temperature and pressure, the GGchem code calculate the various molecules and condensates forming by minimizing the Gibbs free energy. In the 1-dimensional case, by repeating this action, the code can generates the various condensates and calculate their abundance for the full temperature range. These types of graphs showing Condensate abundance vs Temperature are called condensation sequences.

2.1 Initial chemical elements

The first step in the initialisation of our experiment is to make a choice regarding the chemical elements entering the primordial composition of the protoplanetary disk. It is one of the three key features that we use in the derivation of the final chemical composition of a planet. The molecules and condensate species generated by the code depends entirely on this choice as GGchem does not include any species (molecules or condensates) containing elements that are not present in the original choice we make. This means that, the more elements we start with, the more molecules and condensates we have for the determination of the condensation sequence. Moreover, as we had no prior information to the exclusion of any of the 24 elements available in the GGchem code, we have chosen to implement all of them, resulting in a total of 552 molecules and 241 condensates.

2.2 Chemical abundance

The output of interest to us of the GGchem code is the condensation sequences that it generates. It gives us the abundance of each condensate from the condensation of the protoplanetary disk at a given pressure and temperature. This will allow us to explore what kind of condensates are formed depending on the initial abundance values.

When looking at planet composition we need to apply another step. We need to find the individual abundance of each of the 24 chemical elements selected in our experiment. Indeed, one of the aim of this paper is to look at the differences in the chemical composition of a hypothetical solid body with ratio of refractory elements varying from the Solar abundance values. After the condensation of the protoplanetary disk, the various condensates still need to go on forming a planet either through core accretion (Pollack et al., 1996) or gravitational instability (Boss, 1997). During the process, pressures and temperatures becomes high enough to break done the condensates. Thus, what interests us is not the specific identity of the condensates (e.g. MgO, FeS, H_2O, ...) that agglomerate into this body but rather the abundance of each of the basic chemical elements (H, He, Li, ...) as well as the ratios of these elements. We are looking for the fraction of the original gas mixture that condensates into a solid body. Does the elements ratios directly convert from the protoplanetary disk to the condensed phase? Therefore, to go from condensate abundances to the individual abundance of each element the law of conservation of mass must be respected. As such, each element abundance can be found by using its stoichiometric number.

If we have a specific abundance c for a given condensate species, and stoichiometric number s_1, s_2 and s_3 for the chemical elements X, Y and Z, respectively such that:

$$X_{s_1} Y_{s_2} Z_{s_3} = c \tag{1}$$

then the individual abundances of X, Y and Z are given by,

$$X = s_1 c \qquad Y = s_2 c \qquad Z = s_3 c \tag{2}$$

3 Initial chemical abundance

3.1 The Hypatia catalog

The second key feature in our experiment in building planets is to know the primordial composition of the protoplanetary disk from which they form. This is no easy task, because only few molecules can be detected from disk observations, and generally the inner part (≈10 AU) is optically thick. This problem can be solved if we assume that the star host is a good proxy for the chemical composition of the original cloud from which both the star and the protoplanetary disk orbiting it are formed. This is actually a good assumption as can be seen in both papers by Thiabaud et al., 2015 and Dorn et al., 2017, where they show that the elements ratios that we are considering are indeed similar within both the host star and its planets.

To associate a given set of stellar abundances to its protoplanetary disk, one needs to have a database readily available. In that regard, we have chosen the Hypatia Catalog (Hinkel et al., 2014) as the source of our data. Its online Database comprises a wide variety of measurements of stellar abundances in the Solar neighborhood (within 150 pc of our Sun) currently comprising a total of 6193 FGKM-type stars, gathered from a wide variety of sources (+190). The Hypatia Catalog lists for each star a number of elements/species, when available, normalised by the Solar abundance values. Throughout our own experiment we will be using the Solar norm of Asplund et al., 2009.

It is an heterogeneous database, as no unique technique has been used in the derivation of the data. For some elements, various sources list different sets of abundances for the same star, sometimes showing a discrepancy from one another larger than the error bar of each individual value. This is quite upsetting as one would expect to obtain the same outcome regardless of one's own choice of experimental method, thus hinting toward an inherent problem in the method used and/or the experimental protocol. An interesting paper by Hinkel et al., 2016 on these discrepancies between research teams shows that these issues in harmonizing the various techniques over the different group might be inherent to the methods themselves as much as the protocol used. However, this is not immediately relevant in the context of our research, as the purpose of this paper is not in investigating the exact abundance values that one star displays with respect to another, but to see the influence of the typical spreads in the ratios of refractory elements (namely Mg, Si and Fe) found in stars in the Solar neighborhood.

Below, Figure 1 represents the spread of these ratios found in the Hypatia Catalog given with respect to the Solar abundance value.

$$\left[\frac{X}{Y}\right] = \log_{10}\left[\frac{X}{Y}\right]_* - \log_{10}\left[\frac{X}{Y}\right]_\odot \tag{3}$$

with, $*$ representing the stellar value and $\odot$ the Solar value. Only main sequence G-type stars have been considered here (1529).

These graphs show that we can and should expect a spread in the ratios of these elements around the Solar abundance values. 20% of the stars show a ratio $|\mathrm{Mg/Si}| > 0.1$, while 33% show a ratio $|\mathrm{Fe/Mg}| > 0.1$. As for the Fe/S ratio, the spread is even more striking. Only 956 out of the 1529 GV-stars studied have a recorded value of sulphur which result in 43% of them showing a ratio $|\mathrm{Fe/S}| > 0.1$.

3.2 The sample of stars

To study how these variations propagate into the cooling protoplanetary disk, and how they affect the condensation of the various elements within, and therefore, the subsequent planet forming bulk, we have

chosen to study six different stars. These stars were picked according to the following guidelines:

- They are GV-type stars.
- They are not found in a binary or higher order stellar system.
- They are registered in the Hypatia catalog with as much chemical abundance data as possible (with a minimum of Mg/Si/Fe/C/O present).
- They are representative of the typical spreads in the elements ratios that we can expect (cf. Figure 1).

The star sample can be seen in Table 1. The values shown are given with respect to the Solar abundance values as follow:

$$[X] = \log_{10}\left[\frac{X}{H}\right]_* - \log_{10}\left[\frac{X}{H}\right]_\odot \tag{4}$$

with, $*$ representing the stellar value and $\odot$ the Solar value. Two stars out of the sample are remarkable. The star denoted 0 is the Sun and serves as reference, and star 6 which is not a Main Sequence star, but a Red Giant[2]. It was decided to include this star in the sample in order to have at least one star displaying more extreme ratios of refractory elements.

The initial set of abundances used in the derivation of the condensation sequence is composed of 24 elements. However, these elements might not be all available in the Hypatia catalog. To remedy this issue, it was decided that any missing metal abundance would be replaced by the median of the depletion/enhancement of the known elements for that star. H and He are kept at the Solar abundace values for all the stars in the sample (cf. Appendix A).

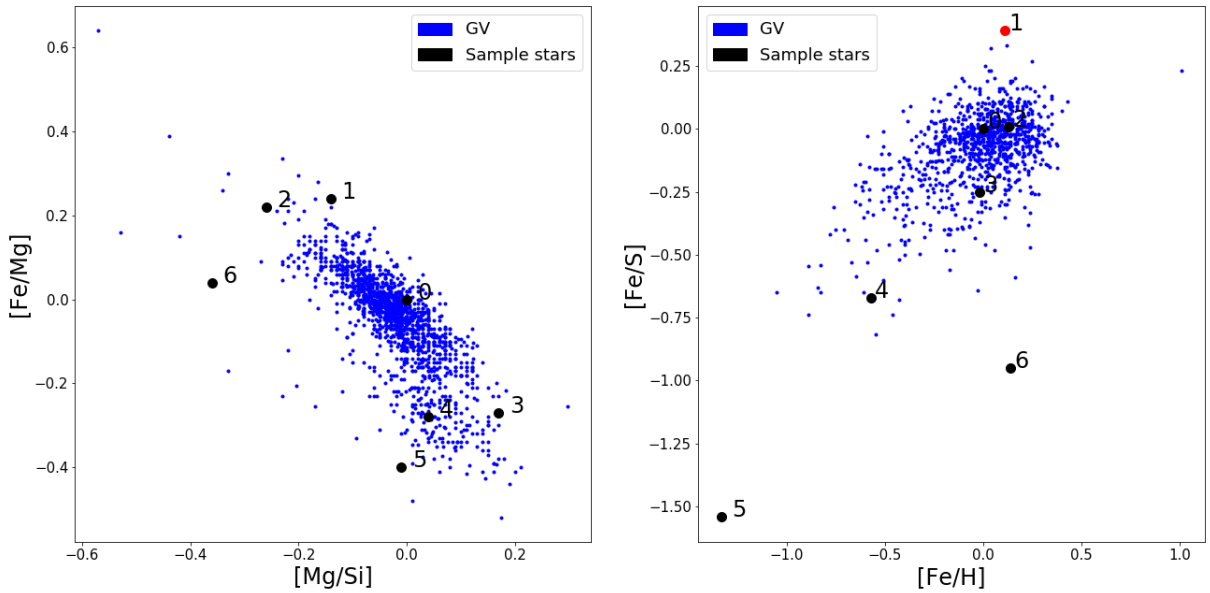

Figure 1: Ratios of the refractory elements Mg, Si and Fe, as well as S, for Main Sequence G-type stars in the Solar neighborhood (within 150 pc of the Sun). Shown as black dots, are the location of the sample of stars studied in this paper and described in Table 1. The red dot indicate a star for which the ratio was not available in the Hypatia Database, and was inferred from the median of the abundance values known (c.f. Appendix A).

[2]HIP 83359 is registered as a G5V star in the Hypatia catalog which does not match its apparent surface temperature. It seems to be an error as Liu et al., 2010 catalog it as a late Red Giant.

#	HIP	Fe	C	O	Mg	Si	Type	Distance[pc]	$T_{\rm eff}$[K]
0	Sun	0	0	0	0	0	G2V	0	5778
1	109836	+0.39	+0.225	+0.25	+0.15	+0.285	G6V	72.8	5810
2	28869	+0.13	+0.01	+0.02	-0.09	+0.17	G0V	47.8	6120
3	63048	-0.019	+0.13	+0.19	+0.25	+0.08	G2V	43.05	5665
4	43393	-0.57	-0.305	+0.03	-0.293	-0.329	G8/K0V	49.67	5306
5	99423	-1.335	-0.49	-0.265	-0.93	-0.92	G0V	109.58	5745
6	83359	+0.145	-0.15	-0.03	+0.1	+0.46	G5-K1III	110.63	4949

Table 1: Main information on the star sample studied in this paper. The full set of chemical abundance used for each star can be seen in Appendix A. Star 0 represents the Sun and is the reference to which any comparison is made. Star 1-5 are Main Sequence G-type stars. Star 6 is separated from the rest to remind us that it is a Red Giant (Type and $T_{\rm eff}$ are from Liu et al., 2010).

4 Pressure-Temperature profile in the disk

The third and last of the key feature in our problem is to decide on a pressure-temperature profile for the GGchem code. As mentioned in Section 2, the code calculates the equilibrium condensation for each of the points of the pT radial disk profile. The specific profile we are modelling is isothermal along the height of the disk, while temperatures cool down along the radius of the disk. Condensates from one part of the disk do not mix with others. The planets we are studying are forming *in situ*.

First of all, we need to determine the inner radius R_0 of the protoplanetary disk. Too close from the host star, the dust grains will sublimate. A brief explanation on that matter is given in Tuthill et al., 2001, where the radius at which dust sublimates is given by,

$$R_0 = \frac{1}{2}\sqrt{Q_R}\left(\frac{T_*}{T_0}\right)^2 R_* \qquad \text{[cm]} \tag{5}$$

with, T_* the surface temperature of the host star, T_0 the sublimation temperature of the dust, and Q_R the ratio of the absorption efficiencies at the given temperatures T_* and T_0.

$$Q_R = \frac{Q(T_*)}{Q(T_0)} \tag{6}$$

Here, $Q_R = 1$ if we assume that the dust grains at the inner rim of the protoplanetary disk are radiating as a black body. Moreover, we will assume a sublimation temperature $T_0 = 1500$ K (H. Kobayashi et al., 2009 and H. Kobayashi et al., 2011), above this threshold most common dust species tend to evaporate.

Given the condition at the beginning of the disk, we can calculate the temperature T as a function of the distance R.

$$T = T_0\left(\frac{R}{R_0}\right)^{-\frac{3}{4}} \tag{7}$$

We need to know the surface density of the disk Σ and the vertical scale height H. The surface density of the protoplanetary disk can be parametrized using the following equation,

$$\Sigma = \Sigma_0\left(\frac{R}{AU}\right)^{-\frac{3}{2}} \qquad \text{[g cm}^{-2}\text{]} \tag{8}$$

with the Minimum Mass Solar Nebula[3] $\Sigma_0 = 1700$ g/cm^2 the normalization constant (Armitage, 2019 and Hayashi, 1981). On the other hand, the scale height is determined by,

$$H = \frac{c_s}{\omega} \qquad \text{[cm]} \tag{9}$$

[3]The Minimum Mass Solar Nebula represents the minimum amount of nebula material that must have been present to form the planets of the Solar system as we know it.

with, c_s representing the sound speed and ω the Keplerian angular frequency (D'Alessio et al., 1998). The sound speed can be calculated easily under the assumption that the disk is isothermal in its height,

$$c_s = \sqrt{\frac{k_B T}{\mu m_p}} \qquad [\text{cm s}^{-1}] \tag{10}$$

with, k_B the Boltzmann constant,$\mu = 2.3$ the mean molecular weight, and m_p the mass of a proton. The Keplerian angular frequency is given by,

$$\omega = \sqrt{\frac{GM_*}{R^3}} \qquad [\text{s}^{-1}] \tag{11}$$

with, G the gravitational constant and M_* the mass of the host star.

Combining Eq. 8, and Eq. 9 the density can be calculated as follow,

$$\rho = \frac{1}{2}\pi\frac{\Sigma}{H} \qquad [\text{g cm}^{-3}] \tag{12}$$

Assuming that the ideal gas law holds, the pressure can be derived as

$$p = \rho\frac{R_c}{\mu N_0 m_p}T \qquad [\text{dyn cm}^{-2}] \tag{13}$$

with, N_0 Avogadro's constant [mol^{-1}], and R_C the ideal gas constant [erg (K·mol)$^{-1}$] (c.f. Figure 2).

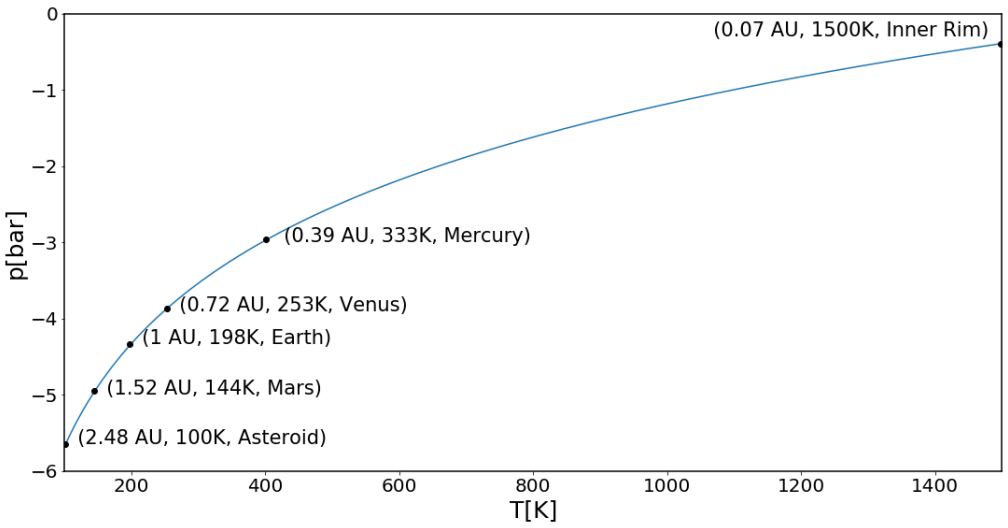

Figure 2: Pressure-Temperature profile of the mid-plane of the protoplanetary disk. Five objects situated at the respective distance of Mercury, Venus, Mars and the Asteroid belt in the Solar System are plotted in black. In this configuration, the host star would be located on the right part of the graph.

5 Results

The key features discussed in the previous section (GGchem code, abundance data, pT-profile) allowed us to derive the condensation sequences for the star sample. These condensation sequences represent a wealth of information and can be overwhelming to read and understand. As such, in this section, we will be focusing on a few interesting aspects of the condensation sequences and redirect the reader to Appendix B for the full presentation of the results.

Two methods are being used in order to investigate the influence of the various elements ratios Mg/Si, Fe/Mg and Fe/S on the composition of forming planets. First of all, we will look at a subset of the condensation sequences (later only referred as subset) of the star sample for the elements Mg and Fe. These graphs display all condensates containing the chemical elements under investigation (all other condensates are removed). The subsets for Si are not shown as the amount of condensates containing this element is too high to really be considered as a subset. However, if a specific condensate of Si is of interest it will be included in the subsets of Mg or Fe.

Secondly, we will be looking at specific solid bodies forming at specific positions in the pT-plane. These solid bodies will represents fictitious planets forming *in situ*. As we have no reason to restrict ourselves to a particular place on the pT-plane, we will look at five hypothetical terrestrial planets forming at the respective distance of Mercury, Venus, Earth, Mars and the Asteroid belt (actually placed at 2.48 AU representing 100 K) in the Solar System. These planets will be labelled with these names to facilitate the subsequent reading.

5.1 Mg subsets

Figure 3 and Figure 4 represent the subsets for the chemical element Mg. If the condensates SiO and SiO_2 appear in the condensation sequence, they are here too. The reason behind this inclusion is that they are influenced by the ratio Mg/Si. In agreement with the findings from Unterborn et al., 2016, a decrease in the Mg/Si leads to a shift from Olivine (Mg_2SiO_4), to Pyroxene ($MgSiO_3$) and eventually Quartz (SiO_2).

Star 3 (Figure 3) displays the highest ratio of Mg/Si (+0.17 dex). At the innermost part of the disk (1500 K), Olivine (black) is the main condensate and stays rather stable in abundance down to 240 K. Subsequently, the cold temperatures allow the condensation of more complex condensates. An interesting point is the absence of any Pyroxene.

Star 4 and 5 (Figure 4) have a Mg/Si ratio of +0.04 dex and -0.01 dex respectively. This second family of stars display a ratio almost equal to that of the Sun and behaves very similarly (compare with the Sun, star 0, Figure 3). Olivine (red in star 4, grey in star 5) is again the main condensate present in the inner part of the disk but a new condensate, SiO (green in star 4, dark green in star 5) appears at the same temperatures. A first shift appears around 1250-1350 K where part of the Olivine and the entire SiO form new condensates including Pyroxene (black). Subsequently, down to around 260 K, the Olivine and Pyroxene compete as the main condensate.

Star 1 (Figure 3) represents somewhat a 'in-between' situation. Its Mg/Si ratio of -0.14 dex leads to an abrupt change in condensates around 1300 K where all the Olivine (red) and SiO (green) disapear and form Pyroxene (light blue) and Quartz (green). However, this happens for a very narrow temperature range for the Quartz, and a somewhat wider one for the Olivine. Below 1200 K, Pyroxene drops in abundance and we have a resurgence of Olivine.

Star 2 (Figure 3) and 6 (Figure 4) display the lowest Mg/Si ratio of the star sample, -0.26 dex and -0.36 dex respectively. This, pushes further the observations made in Star 1. All the Olivine (grey) converts into Pyroxene (black) and all the SiO (green) to SiO_2 (dark green). The main difference being that the Quartz now survives for an extended range of temperatures, down to 470 K for star 2 where it is converted into more complex condensates and reemerge as Quartz at 180 K. For star 6, the disappearance of the Quartz observed between 470 K and 180 K happens for a narrower range of temperatures. Quartz actually only disappears from the subset briefly around 200K.

5.2 Fe subsets

The subsets of Fe are striking in their simplicity (relative amount of condensate species) when compared to those of Mg. Fe is one of the few elements that is found in a solid phase in the inner rim of the protoplanetary disk (1500 K), for all stars in the sample. Moreover, it is always found as one of the most abundant species.

The first, more complex, condensate that forms from metallic Fe is FeS. This shift happens, around 700±15 K, depending on the star of the sample. One exception to this rule is star 6 (Figure 6), where it happens at 858 K. Given the Fe/S ratio (Appendix A), we notice a clear relation between the decrease in the ratio with respect to the speed at which FeS forms, as well as the subsequent allowed condensate phase of Fe.

From star 1 to star 6 the Fe/S ratio decreases. A lower ratio represents more S atoms readily available to bind with Fe. When the right temperature is reached, they start to bind and form FeS. The more S available, the quicker Fe gets depleted from the condensation sequence. As a matter of fact, in star 0 to 3 (Figure 5), the depletion of iron is a relatively slow process which accelerate abruptly (leading to the total disappearance of metallic Fe) only when other Fe-condensates form.

Star 4, 5 and 6 (Figure 6), which are associated with the lowest Fe/S ratios of the star sample show the most extreme behaviors. The amount of S readily available is such that virtually all the metallic Fe (black) condensates in an instant and stay stable as FeS (blue) until colder temperatures are reached. At these temperatures ranging from 321K to 279K depending on the star under consideration, FeS combined further with S leading to the final form of Fe as FeS_2 (grey). As a matter of fact, the phase transition between this three condensates species is relatively smooth, with no noticeable change in the original abundance of metallic Fe.

This leads to the division of the star sample into two groups. One group with a Fe/S ≥ -0.25 dex that forms, at low temperatures, other Fe-condensates than FeS and FeS_2 (Figure 5) and another group with a Fe/S ≤ -0.67 dex forming only these two iron-sulphur alloys (Figure 6).

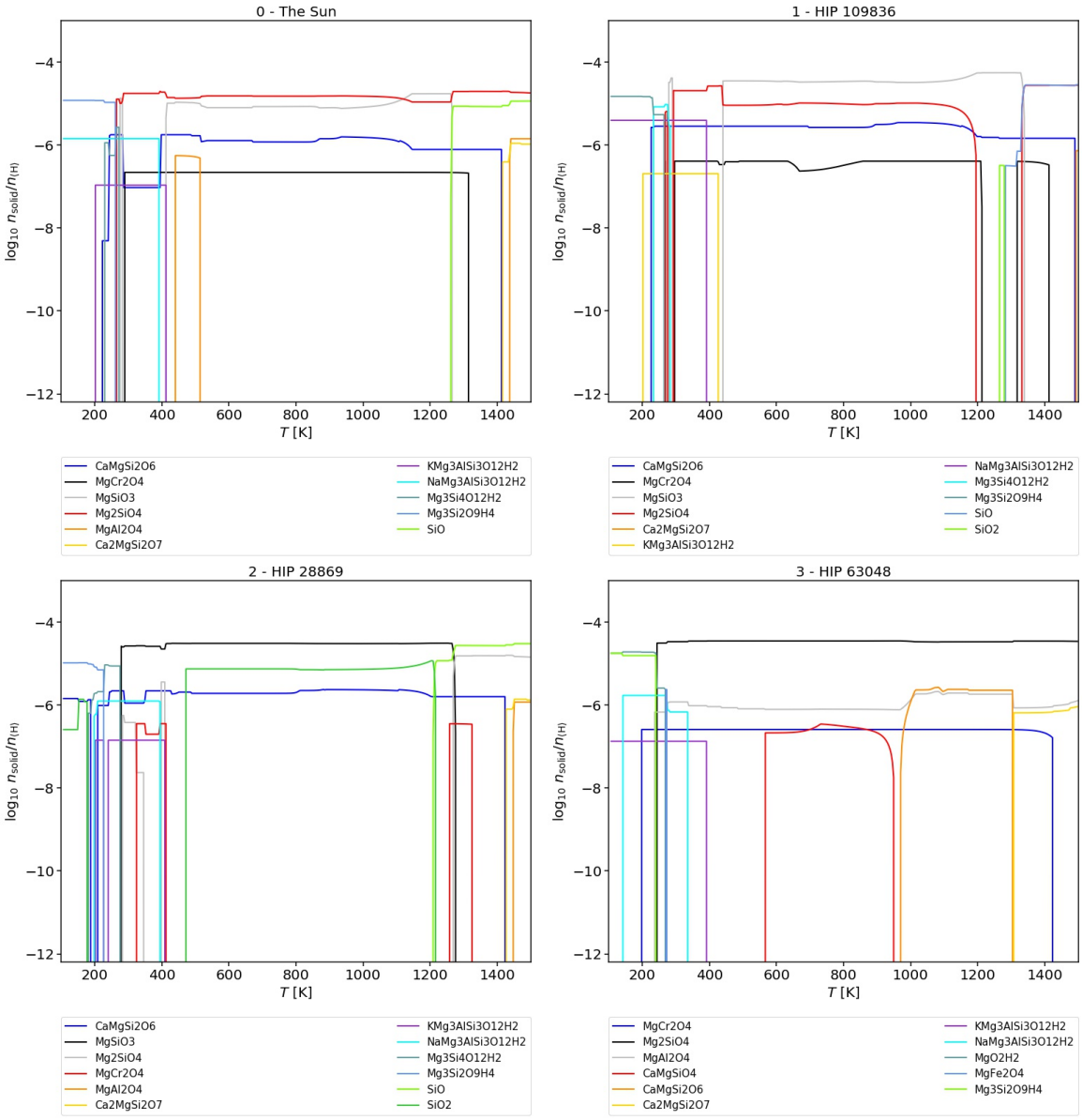

Figure 3: (Star 0, 1, 2 and 3) Mg-subsets represented for each of the stars from the sample. The full condensation sequences can be found in Appendix B. All condensates containing the element Mg are represented, while the remaining condensates are removed. One exception to this rule apply to the condensates SiO and SiO_2, which are represented if present in the condensation sequence. Each number and name attached to the graphs follow the formalism used all throughout this paper and found in Table 1.

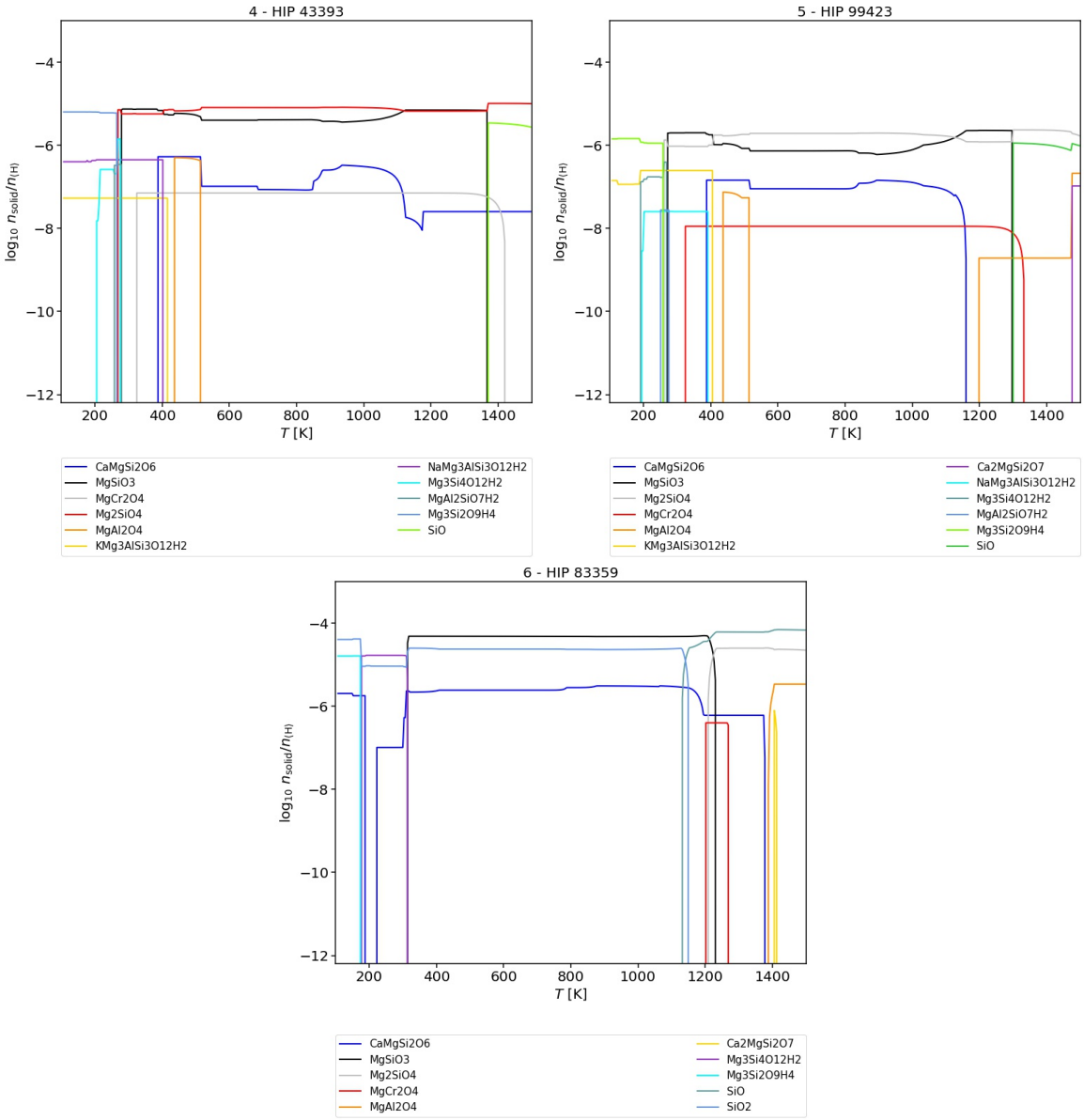

Figure 4: (Star 4, 5 and 6) Mg-subsets represented for each of the stars from the sample. The full condensation sequences can be found in Appendix B. All condensates containing the element Mg are represented, while the remaining condensates are removed. One exception to this rule apply to the condensates SiO and SiO_2, which are represented if present in the condensation sequence. Each number and name attached to the graphs follow the formalism used all throughout this paper and found in Table 1.

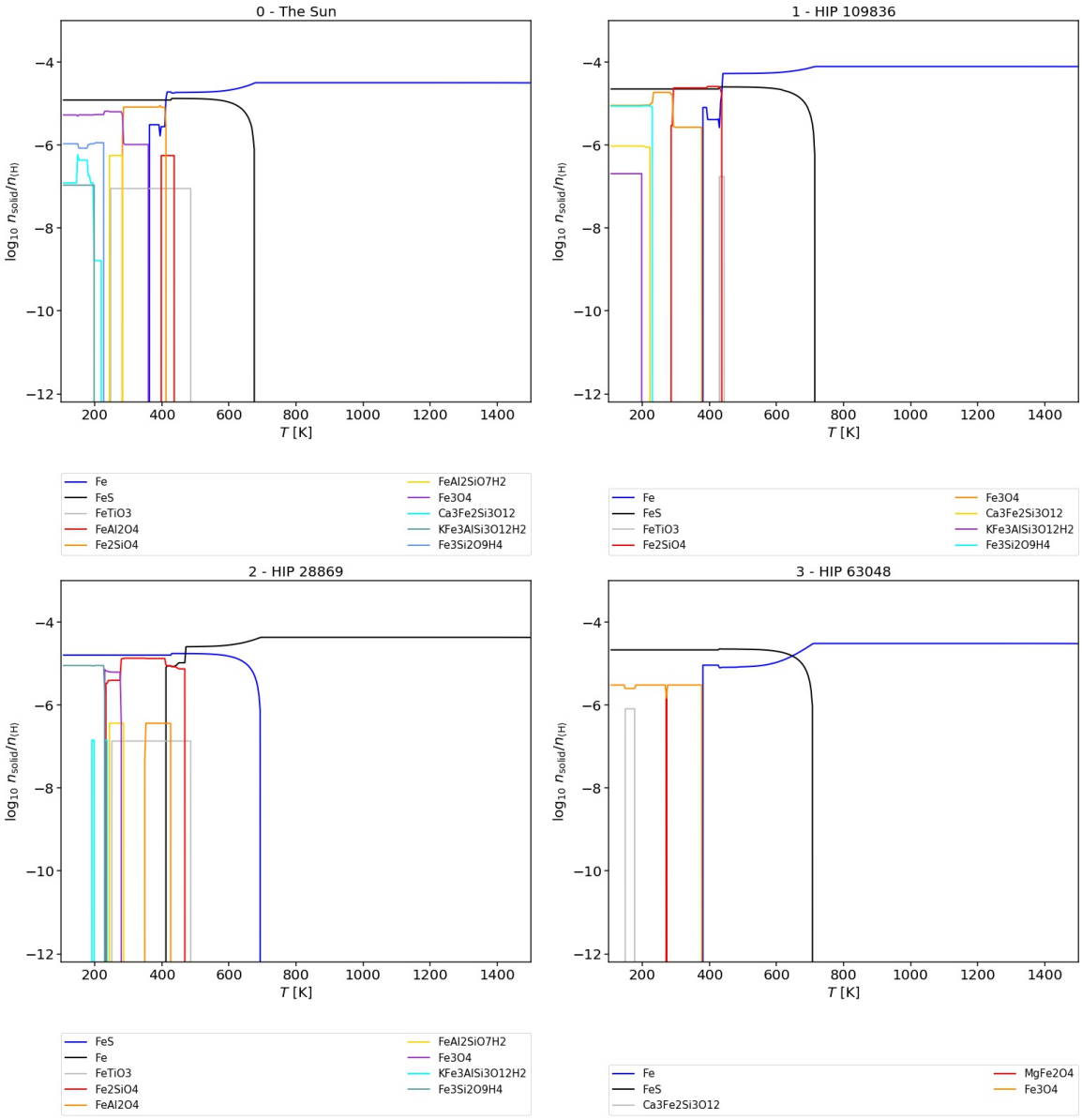

Figure 5: (Star 0, 1, 2 and 3) Fe-subsets represented for each of the stars from the sample. The full condensation sequences can be found in Appendix B. All condensates containing the element Fe are represented, while the remaining condensates are removed. Each number and name attached to the graphs follow the formalism used all throughout this paper and found in Table 1.

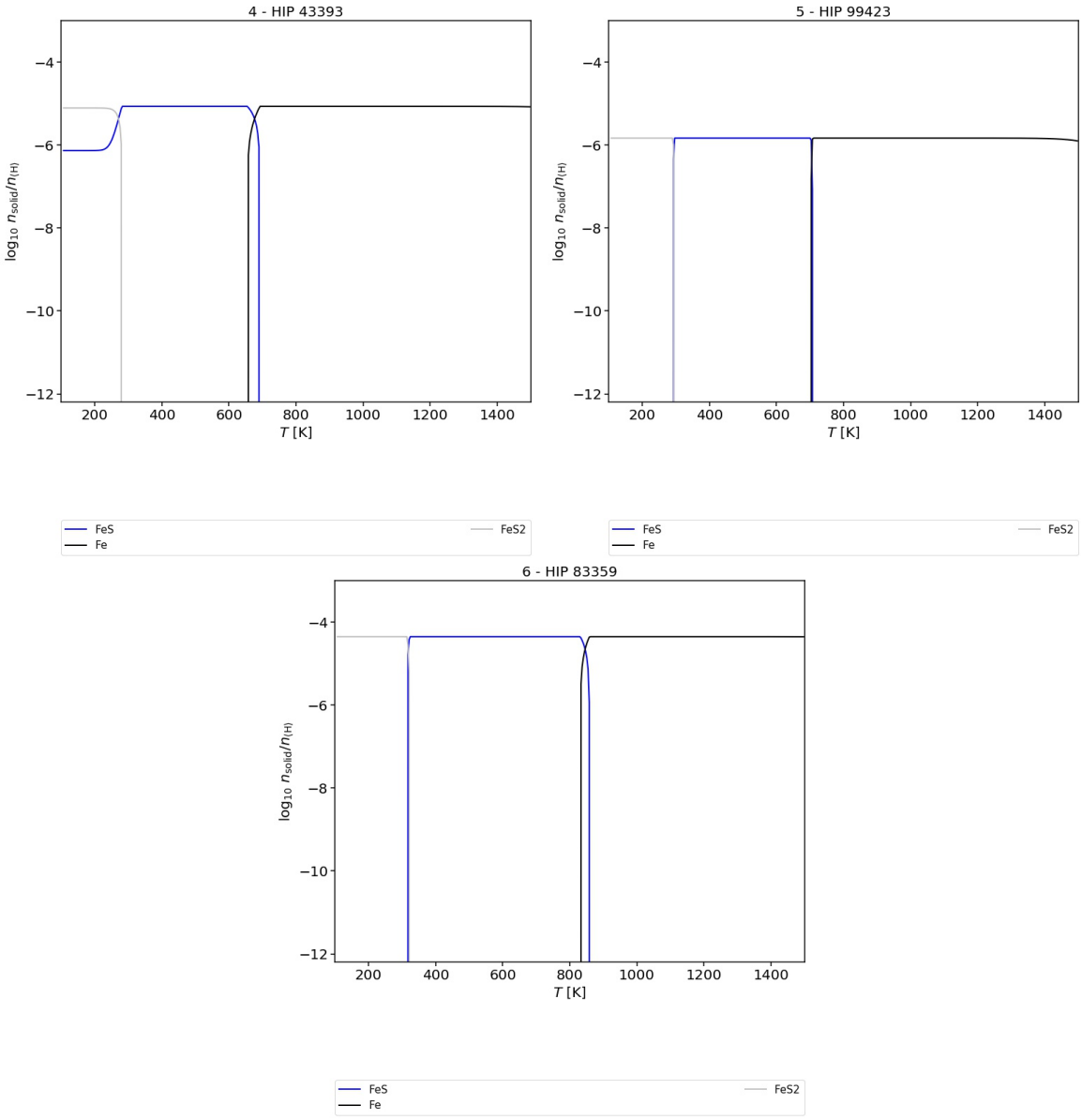

Figure 6: (Star 4, 5 and 6) Fe-subsets represented for each of the stars from the sample. The full condensation sequences can be found in Appendix B. All condensates containing the element Fe are represented, while the remaining condensates are removed. Each number and name attached to the graphs follow the formalism used all throughout this paper and found in Table 1.

5.3 Planet composition

In the following section we display the impact of changing the ratios Mg/Si, Fe/Mg and Fe/S on the five hypothetical planets forming at the distances of Mercury (0.39 AU), Venus (0.72 AU), Earth (1 AU), Mars (1.52 AU) and the Asteroid belt (2.48 AU) in the Solar System. Figure 7 displays these results as mass fraction (wt%) vs the host star under consideration (Table 1). The numerical values associated to these graphs can be found in Appendix C. Figure 8 shows the propagation of various chemical ratios from the gas phase to the condensed phase. Ratios of oxygen with respect of the refractory elements can help us in understanding the boundary between an oxidized or reduced interior, while Fe/S can help us understand the S wt% present in the core.

5.3.1 Oxygen

Oxygen mass fraction has a very interesting behavior. For the exception of the two body pass the snow line[4] (Mars and Asteroid), neither the planet under consideration, nor the host star seem to have a significant influence on the mass fraction of O. Mercury has a total difference (from the minimum value attained to the maximum value) of 4.93%, Venus 6.41 %, Earth 6.65 %, Mars 43.49 % and Asteroid 39.58 %. However, slight changes are observed within a stellar system from planet to planet. There is a tendency to have an increase O wt% as one goes further away from the host star (colder temperatures). One exception is star 6, with a lower O wt% for Venus and Earth with respect to Mercury.

The large difference found in the O wt% for Mars and Asteroid is directly linked to their formation happening passed the snow line. As one can see from the Appendix B, a large abundance of water is forming leading to an increase of O in its condensate form.

5.3.2 Magnesium and Silicon

Magnesium and silicon are two chemical elements intricately linked. As can be seen from Figure 3 and 4, these two elements, in association with other metals, form various condensate species. Moreover, we saw in Section 5.1, that the Mg/Si ratio had an influence on the formation of silicates and quartz condensates.

Magnesium follows the behavior shown by the Mg/Si ratio. When this ratio decreases so does Mg, and *vice versa*. Silicon behaves somewhat more erratically, not reflecting the same changes observed in Mg. The Mg/Si ratios of the gas phase (Appendix A) can be divided into three families. Star 3 with a high ratio (+0.17 dex), stars 0, 4 and 5 with a ratio equal or close to Solar ($\approx$0 dex), and stars 1, 2 and 6 with a low ratio ($\leq$-0.14 dex).

These three families are very well represented in the Mg graph for Mercury, Venus and Earth. Mars and Asteroid behaving similarly for the most part but showing discrepancies with respects to the other planets more noticeable for the case of star 4, 5 and 6. While the most inner three planets show a stable behavior for star 4 and 5, and a subsequent clear decrease with star 6. Mars and Asteroid show a decrease between star 4 and 5, followed by a clear increase in Mg wt% in star 6. This is due in part because of the O wt% of these two planets. This high value with respect to the inner three rocky planets, induces the mass fraction of other elements to be reduced to low percents.

For the case of Si, the three families of ratios previously described are blurred and it is difficult to find any pattern related to the Mg/Si ratio. The behavior of Mg and Si tend to show that, the mass fraction of Mg is directly impacted by the Mg/Si ratio. Fluctuations in the ratio reflecting the fluctuations in the abundance of Mg atoms able to condensate. Whereas the condensation of Si does not strictly follow this behavior and seems to be impacted by other mechanics not taken into account in this research.

5.3.3 Iron and Sulphur

Iron is a very important chemical element as its heavy weight will lead it to sink to the center of the condensing planet to form its core. However, the core is not only made out of Fe. The lower density of

[4]The snow line represents the distance from the host star where the temperature is cold enough for volatile elements such as water to condensate.

the core with respect to what one would expect from Fe at these temperatures and pressures indicates the presence of lighter elements. As a matter of fact Birch, 1952 shows that the core is composed than more than iron. In recent years (Hirose et al., 2013), sulphur became a prime candidate to identify these lighter Fe-alloy present in the core. Therefore, the behavior of Fe and S is relatively important to describe not only the size of the core, but also the percentage of lighter alloys present in it.

A clear relation between the Fe/S ratio and sulphur can not easily be drawn from our results. The variations in the ratio does not impact the mass fraction of S as it does for Fe. That is because after S binds with metallic-Fe it will go on forming other sulphuric condensates that are impacted by other elements ratios (c.f. Appendix B). However, the previous results found in Section 5.2 help us understand these results. Star 0 to 3 show the lowest mass fraction (<10 %), which corresponds to the group of stars with the highest ratio Fe/S ≥ -0.25 dex, while star 4 to 6 show the highest mass fraction which corresponds to the group of star with the lowest ratio Fe/S ≤ -0.67 dex.

On the other hand the Fe/Mg ratio has a clear impact on the size of the core. The higher the ratio, the higher the Fe wt%. Star 6 behaving differently, as its near Solar ratio (+0.04) would lead us to expect similar results as star 0, but are lower for the three inner most rocky planets. However, Mars and Asteroid do behave as we would expect.

5.3.4 Chemical elements ratios in the condensed phase

An important point in our investigation of planet composition is to know how the initial various chemical ratios present in the protoplanetary disk (the gas phase) propagate to the condensed phase from which the planets form. Because chemical elements do not condensed at the same temperatures, nor the same rate depending on the distance from which a planet form from its host star, these ratios may variate leading to important internal changes. Figure 8 represents various ratios found per planet and depending on the host star considered. The results are normalised by the Solar abundance values as was presented in Eq 3.

Refractory elements such as Fe, Mg and Si are fully condensed at the formation temperatures of the five bodies under investigation. Therefore, the ratios Fe/Si, and Mg/Si (Figure 8) are found back in the condensed phase for all planets. This is not the case when one looked at ratios involving more volatile elements such as oxygen and sulphur.

The ratios involving O (Fe/O, Mg/O and Si/O) tend to show the same behavior. The three innermost rocky planets are forming at temperatures where a part of the oxygen is still present in the gas phase, and as such end up forming from a condensed phase with higher oxygen ratios, while the two bodies passed the snow line end up with ratio equal to that of the initial gas phase.

The Fe/S behaves similarly to that of oxygen but in a more unstable fashion. While the snow line for oxygen happens for roughly the same temperature in each stellar system, leading to the distinction between three planets within its boundary and two passed it, the condensation of sulphur is more dependent on the stellar system. We notice that the group identified in Section 5.2, as forming other condensates than FeS/FeS_2 (Figure 5), shows a ratio Fe/S in the condensed phase equal to that of the gas phase, regardless of the planet chosen. However, in the second group (Figure 6) the 'sulphur line'[5] is being pushed away from the host star. In star 4, Earth, Mars and Asteroid have the same Fe/S ratio as the one found in the initial gas phase, while in star 5 and 6 only Asteroid shows this behavior. This behavior is directly linked to the capacity of S atoms to form other sulphuric condensates. The prime example being Asteroid in star 5. The extreme difference in the Fe/S ratio comes from the formation at T< 150 K of NH_4SH in large abundance. Therefore, the lower the Fe/S ratio is, the more S atoms are available to form more complex condensates at low temperatures, the more the 'sulphur line' is found to be at low temperatures.

[5]The distance at which all the S condensed.

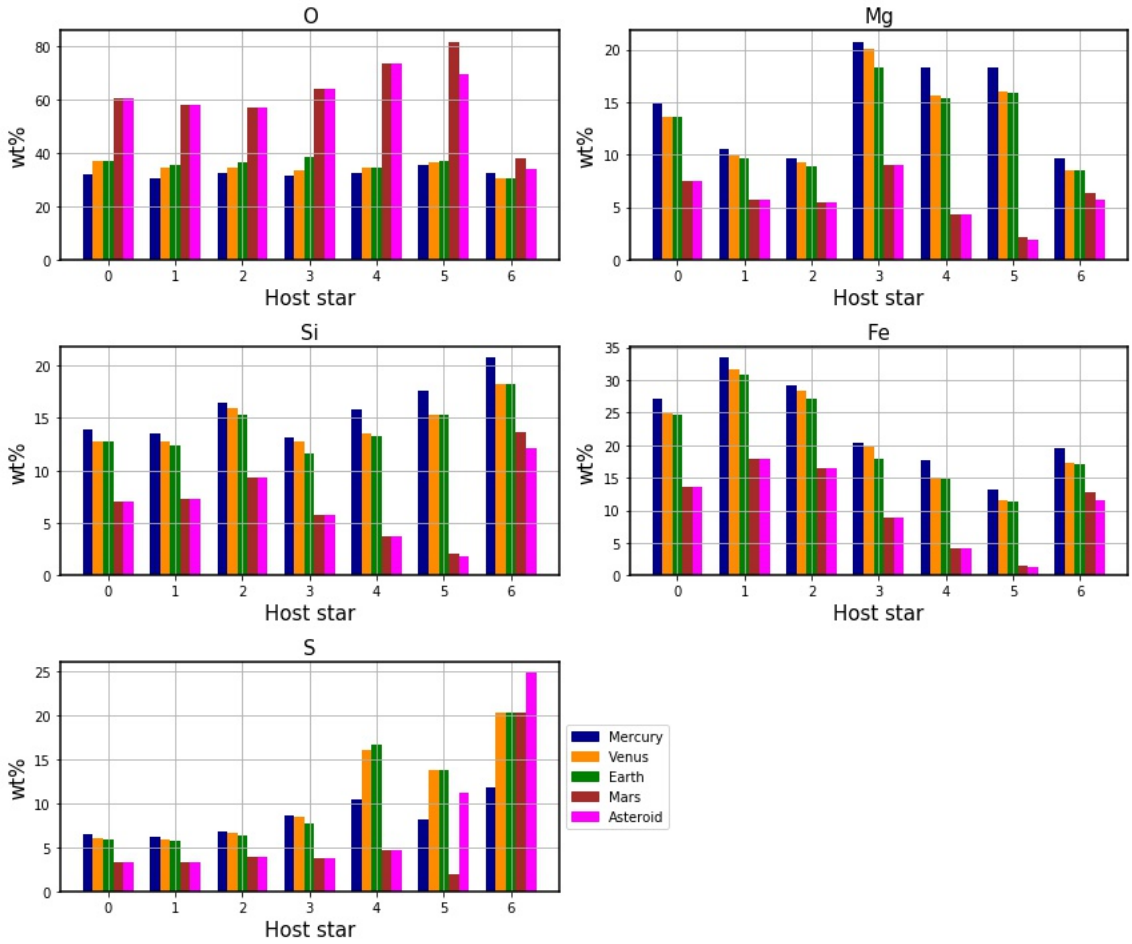

Figure 7: Mass fraction of five bodies forming *in situ* at the respective distance of Mercury (blue), Venus (yellow), Earth (green), Mars (red) and the Asteroid belt (purple) in the Solar System. Values are given on the y-axis as percentage of the total mass of the body [wt %] (c.f. Appendix C). The x-axis labelled from 0 to 6 represents the host star where the planets formed.

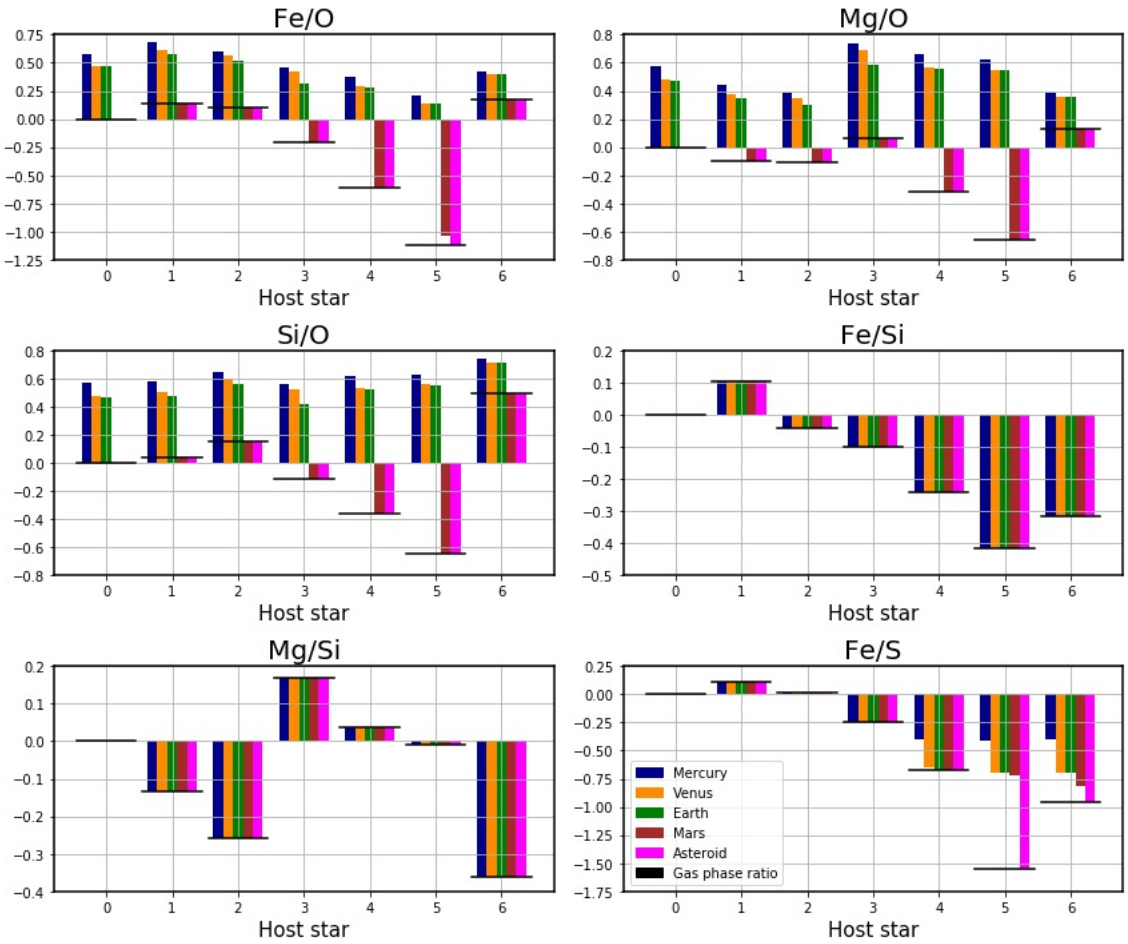

Figure 8: Elements ratios found in the condensed phase from which five fictitious planets form *in situ* at the respective distances of Mercury (blue), Venus (yellow), Earth (green), Mars (red) and Asteroid (purple) in the Solar System. The x-axis labelled from 0 to 6 represents the host star. Ratios are normalised by the Solar abundance values (Eq 3). A full report on these ratios is given in Appendinx D.

6 Discussion

The condensation sequences are a very interesting tool to use in order to analyse what type of condensates one form on the basis of the initial abundance of each chemical elements. We have seen that slight changes in the Mg/Si ratio results in differences in Olivine, Pyroxene and Quartz abundances, that the Fe/Mg ratio influenced the size of the planet's core or that the Fe/S ratio dictate the possible condensates that Fe can form. However, it is important to remember that the condensation sequences are generated by the GGchem code for a specific pressure-temperature profile. It calculates the abundance of the condensates to expect when an initial cloud cools down. For the purpose of planet building, an extra step is needed. These condensates need, either through core accretion (Pollack et al., 1996) or gravitational instability (Boss, 1997), to form the final planet. In the process, temperatures and pressures increase such that the identity of the condensate species is lost. What remains is the individual chemical elements. To draw more conclusions about the final planet structure on the basis of the initial refractory ratios found in the cloud, one would need to model the accretion and subsequent cooling of the planet. However, the condensation sequences are still a good approximation as to what to expect as the ratios of the refractory elements Mg/Si and Fe/Si (Figure 8) are found back into the condensate phase from which the planets form (no Fe nor Mg remain in the gas phase after T<1000 K). However, this is not the case for more volatile elements such as oxygen and sulphur. They can remain, in some cases, almost fully in the gas phase down to low temperatures. As some of the fictitious planets under consideration form at temperatures higher than that, they will have an initial Fe/S or Fe/O ratio (in the condensate phase) higher than the one found in the original gas phase which will results in different condensation sequences.

Both the mass fraction and the ratios of the various chemical elements in the condensed phase are important in understanding what type of planets are forming. The composition of the core will influence its size, the magnetic field of the planet or change the heat flow from the core to the surface. The apparent density deficit of the inner and outer core leads scientists to think that the core is composed to more than Fe (Birch, 1952). A few elements are under consideration and Table 1 of Hirose et al., 2013 is very interesting in that regard as it repertory the mass fraction of Si, O, S, C and H that might be present in the core from various sources. Possible S wt% range from 0% to 13% depending on the source. A large fraction of the core can then be composed of S. Given that the Fe/S seems to influence, in some cases drastically, the S wt% we can wonder on the type of planet forming. Star 6 is the most striking example. Its Fe/S ratio leads it to only form from metallic Fe, FeS and FeS_2 leading to planets (except Mercury) having a larger S wt% than Fe wt %. If indeed, the deficit in the inner and outer core can be attributed to these elements sinking into the core, depending on how much of S actually sink in, it would lead sulphur to be the predominant element in it. Such planets would be oddities. This leads us to ask ourselves how reliable are the initial sulphur abundance used to run the GGchem code. These were taken from the Hypatia catalog, and as mentioned in Section 3, the various data collected in the Hypatia Database are from various sources. The values are actually the median of all recorded sources, which in some cases, show discrepancies from one another larger than the error bar of each individual value. In their paper Hinkel et al., 2016 show that derivation of stellar abundance is no trivial exercise and leads to discrepancies that cannot only be explained by the protocols used by the different teams. It is important to remember that fact when reviewing our results.

It is interesting to see that the initial ratios found in the protoplanetary disk directly translate to the condensed phase for the ratios of the refractory elements (Figure 8). This is true because no more Mg, Fe or Si are present in the gas phase. Planets that would form much closer to the star, at higher temperatures, would have different ratios of refractory elements. However, this is not the case for ratios with respect to more volatile elements. Fe/O, Mg/O and Si/O are good indicator when it comes to study if the planets interior is reduced or oxidized. The assumption that an elements ratio directly translate from the gas phase to the condensed phase is not true. Most of the rocky planets studied show a higher ratios due to the depletion of O in its condensed form. This means that calculations of planets interior using the ratios of the gas phase will have a tendency to result in more oxidized interior than they are.

The same applies to sulphur and might as well explain some of the extreme results found earlier on the S wt% in the core. For the most extreme cases, star 5 and 6, the Fe/S ratios in the gas phase (Appendix A) underestimate the actual ratios of the condensed phase for most of the planets. Which means that less

sulphur will be available when the planets actually goes through its accretion process. The new condensation sequence should show less FeS and FeS_2, and might as well show the presence of other Fe-condensates. This would change the possible lighter elements and their abundance found in the core.

7 Conclusion

In this research we have set to investigate the influence of the equilibrium condensation sequence for various element mixtures using the GGchem code when the ratios of the refractory elements Mg, Si and Fe are changed from the Solar abundance values. We have studied this influence for the protoplanetary disk of five Main Sequence G-type stars and one Red Giant. We have found that changing the Mg/Si ratio has a direct impact on the type of silicates formed from the condensation, with a shift from Olivine (Mg_2SiO_4) and SiO to Pyroxene ($MgSiO_3$) and Quartz (SiO_2) when the Mg/Si ratio diminishes. Furthermore, the Fe/S leads to two type of condensation sequences. For Fe/S≥ -0.25 dex, metallic-Fe forms various type of condensates at low temperatures while for Fe/S≤ -0.67 dex, metallic-Fe only forms FeS and FeS_2. This was an interesting experiment, as one can see that changes within the typical spreads of these ratios (Figure 1) leads to clear distinction in the condensates.

Subsequently, from the results of these condensation sequences we have investigated the composition of planets forming around the sample of stars. The Fe/Mg ratio impact the size of the core of a planet with a higher ratio leading to a bigger core size. Moreover, Fe/S ratio impact the S wt %.

We found that assuming that the elements ratios from the gas phase directly translates to the condensed phase is not always true. Refractory elements condensed at higher temperatures, and therefore their elements ratios are found back in the condensed phase. However, ratios of volatile elements depends at which temperature a planet form. Oxygen only fully condensed passed the snowline, and as such, any planet forming within this boundary will have a higher ratio. This is important as it will lead to planets having more reduced interior.

In conclusion, our study show that typical spread in main sequence G-type star does impact significantly the outcome of planet formation. When studying the composition of a forming planet, the elements ratios of the condensed phase need to be calculated from the condensation of the protoplanetary disk, modelled from the specific abundance of the stellar system under investigation.

A Initial chemical abundances (gas phase)

#	HIP	H	He	Fe	C	O	Mg	Si	Ca
0	Sun	0.0	0.0	0.0	0.0	0.0	0.0	0.0	0.0
1	109836	0.0	0.0	+0.39	+0.225	+0.25	+0.15	+0.285	+0.22
2	28869	0.0	0.0	+0.13	+0.01	+0.02	-0.09	+0.17	+0.1
3	63048	0.0	0.0	-0.019	+0.13	+0.19	+0.25	+0.08	+0.13
4	43393	0.0	0.0	-0.57	-0.305	+0.03	-0.293	-0.329	-0.44
5	99423	0.0	0.0	-1.335	-0.49	-0.265	-0.93	-0.92	-1.02
6	83359	0.0	0.0	+0.145	-0.15	-0.03	+0.1	+0.46	+0.26

#	HIP	Ti	Li	N	F	Na	Al	P	Cl
0	Sun	0.0	0.0	0.0	0.0	0.0	0.0	0.0	0.0
1	109836	+0.285	+0.277	+0.29	+0.277	+0.415	+0.19	+0.277	+0.277
2	28869	+0.18	+0.12	+0.12	+0.12	-0.02	-0.08	+0.12	+0.12
3	63048	+0.11	+0.06	+0.095	+0.095	+0.08	+0.23	+0.095	+0.095
4	43393	-0.21	−0.305	−0.305	−0.305	-0.46	-0.263	−0.305	−0.305
5	99423	-1.065	+1.18	+0.37	−0.873	-1.41	-0.825	−0.873	−0.873
6	83359	+0.13	+0.145	+0.185	+0.185	+0.46	+0.38	+0.185	+0.185

#	HIP	K	V	Cr	Mn	Ni	Zr	W	S
0	Sun	0.0	0.0	0.0	0.0	0.0	0.0	0.0	0.0
1	109836	+0.277	+0.25	+0.27	+0.33	+0.38	+0.277	+0.277	+0.277
2	28869	+0.12	+0.27	+0.21	+0.12	+0.14	+0.12	+0.12	+0.12
3	63048	+0.095	+0.06	+0.07	+0.02	+0.036	+0.23	+0.095	+0.23
4	43393	−0.305	-0.27	-0.49	-0.73	-0.56	-0.2	−0.305	+0.1
5	99423	+0.36	-0.95	-1.29	-0.52	-1.34	+1.045	−0.873	+0.21
6	83359	+0.185	+0.17	+0.26	+0.2	+0.23	-0.16	+0.185	+1.1

#	HIP	Mg/Si	Fe/Mg	Fe/S
0	Sun	0.0	0.0	0.0
1	109836	-0.14	+0.24	+0.11
2	28869	-0.26	+0.22	+0.01
3	63048	+0.17	-0.27	-0.25
4	43393	0+.04	-0.28	-0.67
5	99423	-0.01	-0.4	-1.54
6	83359	-0.36	+0.04	-0.96

Table 2: Full report on the initial chemical abundances in the gas phase for the stars investigated in this paper (24 chemical elements). These values are normalised with respect to the Solar abundance value as described by Eq. 4. H and He are kept at the Solar abundance values for all stars while metals are specific to the star. In black are the values from the Hypatia catalog, while the red values are elements missing abundances in the database and the values have been approximated using the median of the known data for the metals of the specific star.

B Condensation Sequence

B.1 The Sun

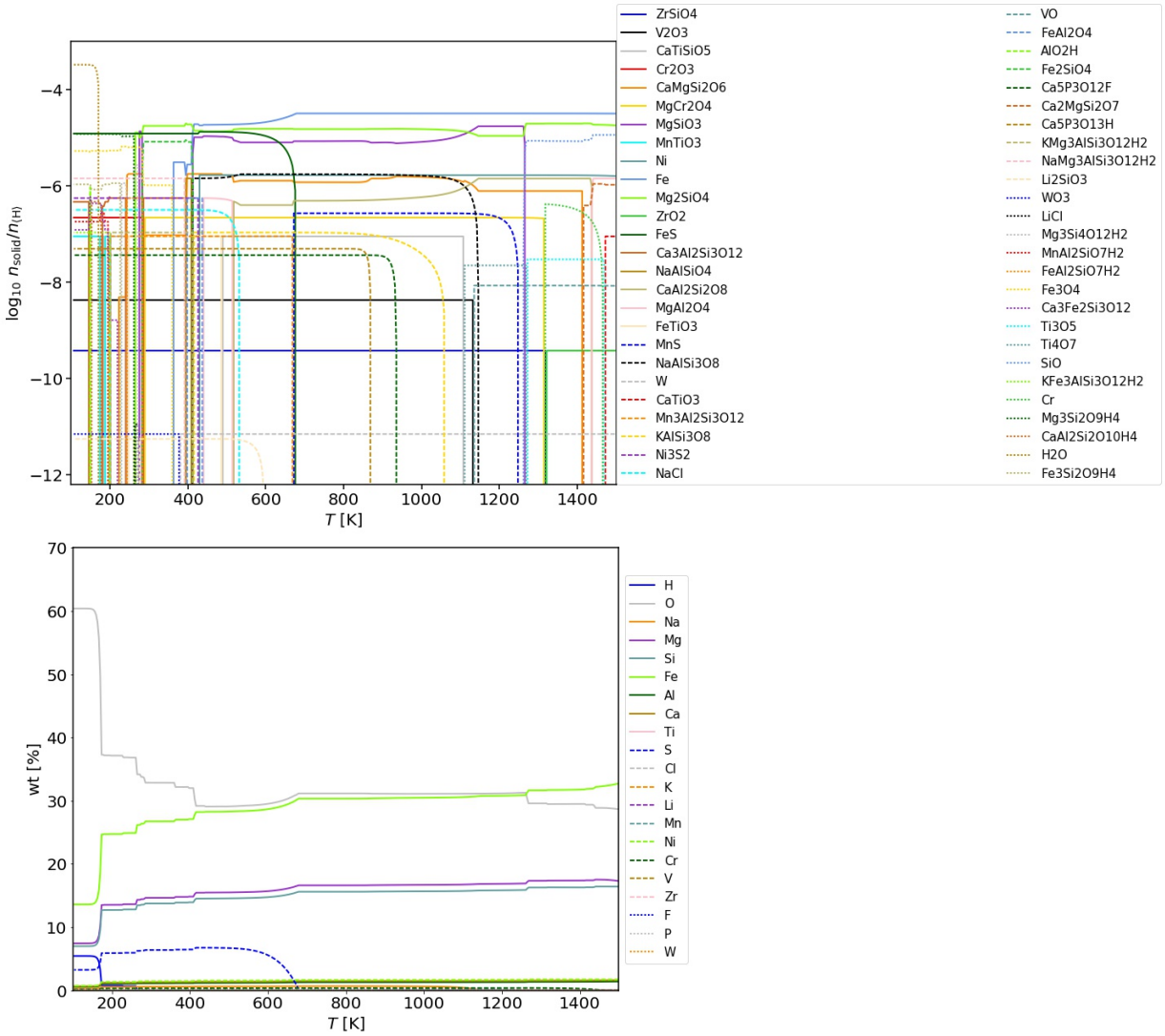

Figure 9: **Upper graph** Condensation sequence for the Sun (star 0). The star is located on the right side of the graph. Smooth condensation (round edge) represent phase transition gas/solid, while sharp condensation represents phase transition solid/solid.
Lower graph The condensation sequence is translated into a graph showing the mass fraction of each element as a percentage.

B.2 HIP 109836

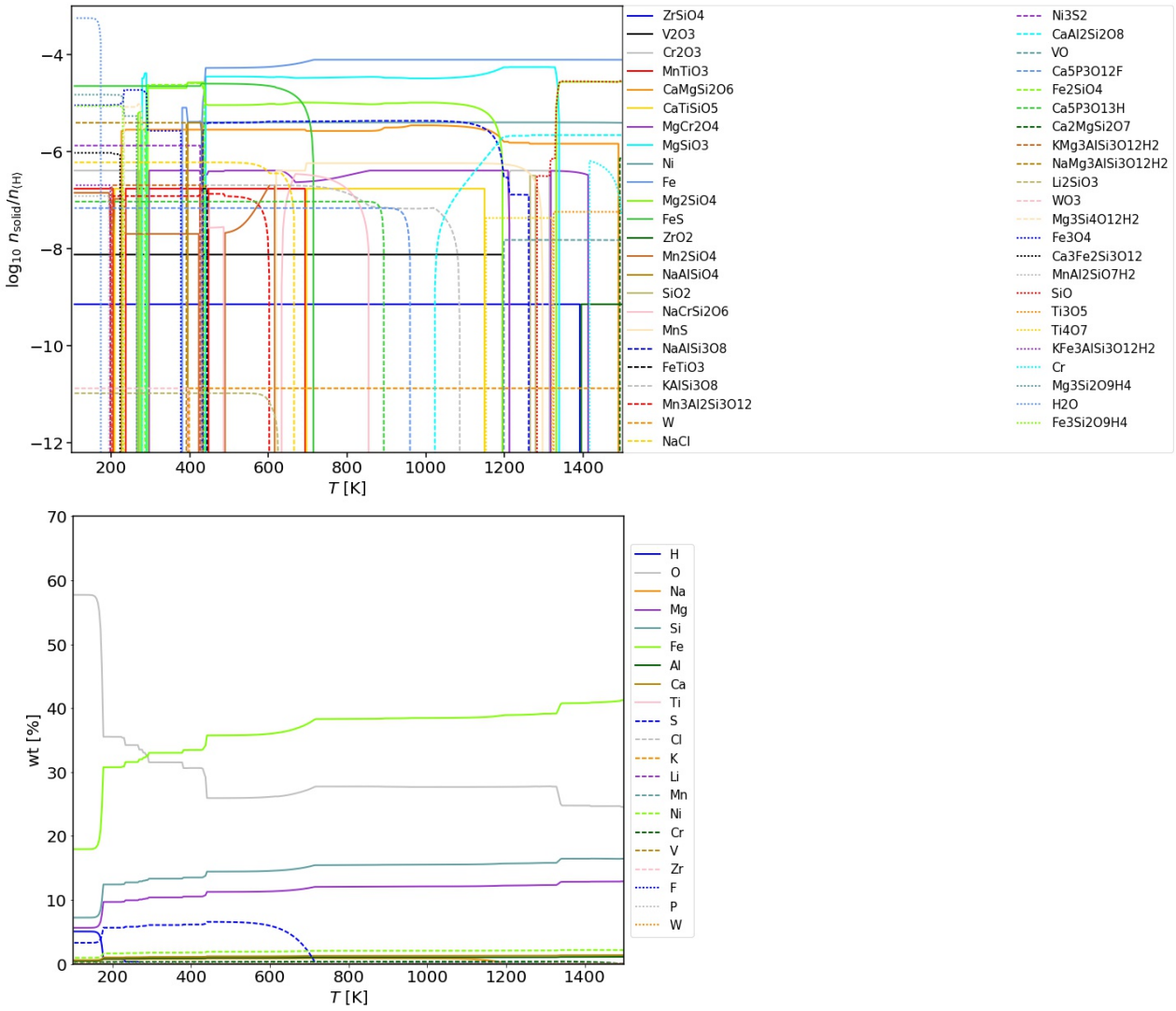

Figure 10: **Upper graph** Condensation sequence for HIP 109836 (star 1). The star is located on the right side of the graph. Smooth condensation (round edge) represent phase transition gas/solid, while sharp condensation represents phase transition solid/solid.
Lower graph The condensation sequence is translated into a graph showing the mass fraction of each element as a percentage.

B.3 HIP 28869

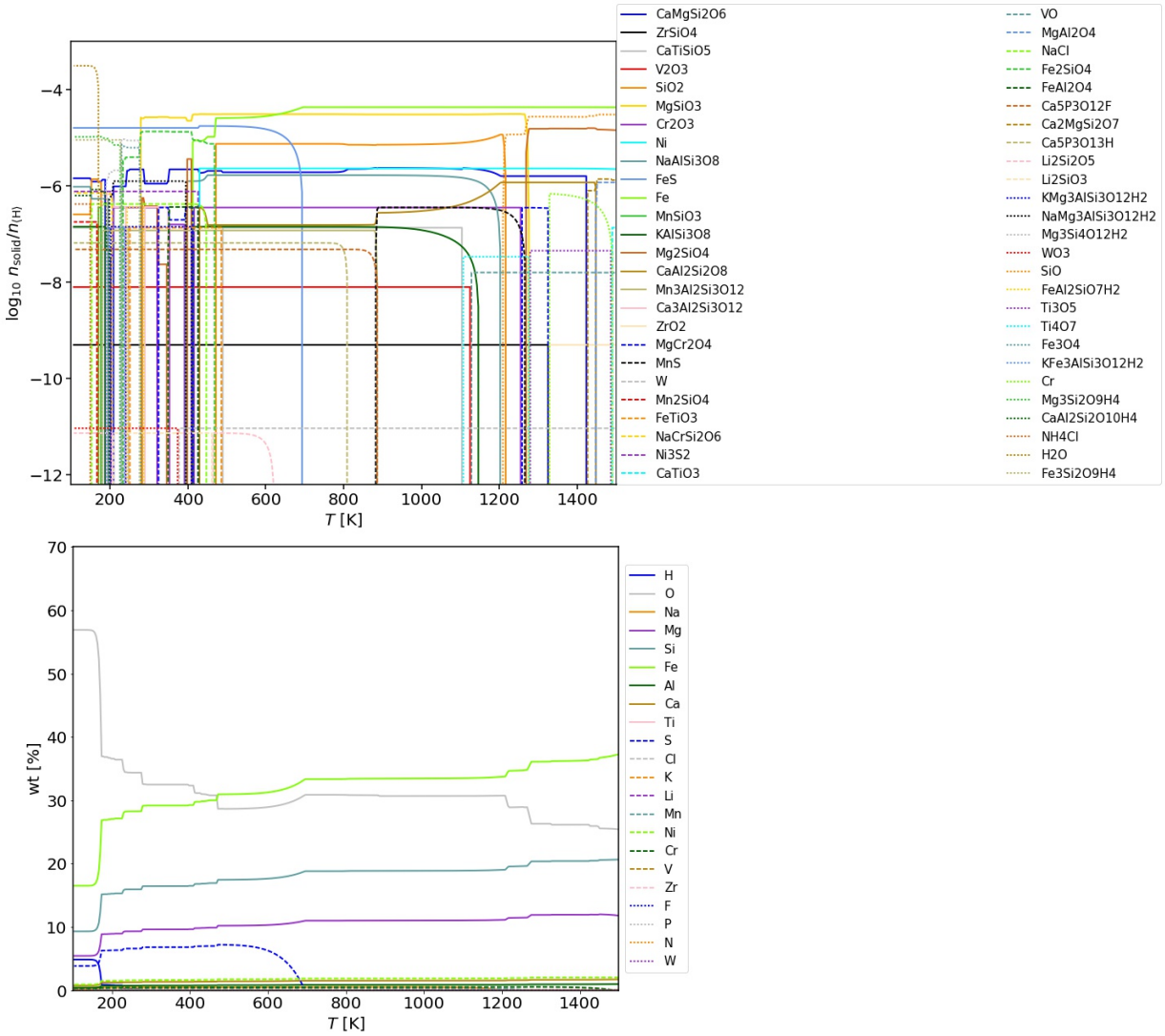

Figure 11: **Upper graph** Condensation sequence for HIP 28869 (star 2). The star is located on the right side of the graph. Smooth condensation (round edge) represent phase transition gas/solid, while sharp condensation represents phase transition solid/solid.
Lower graph The condensation sequence is translated into a graph showing the mass fraction of each element as a percentage.

B.4 HIP 63048

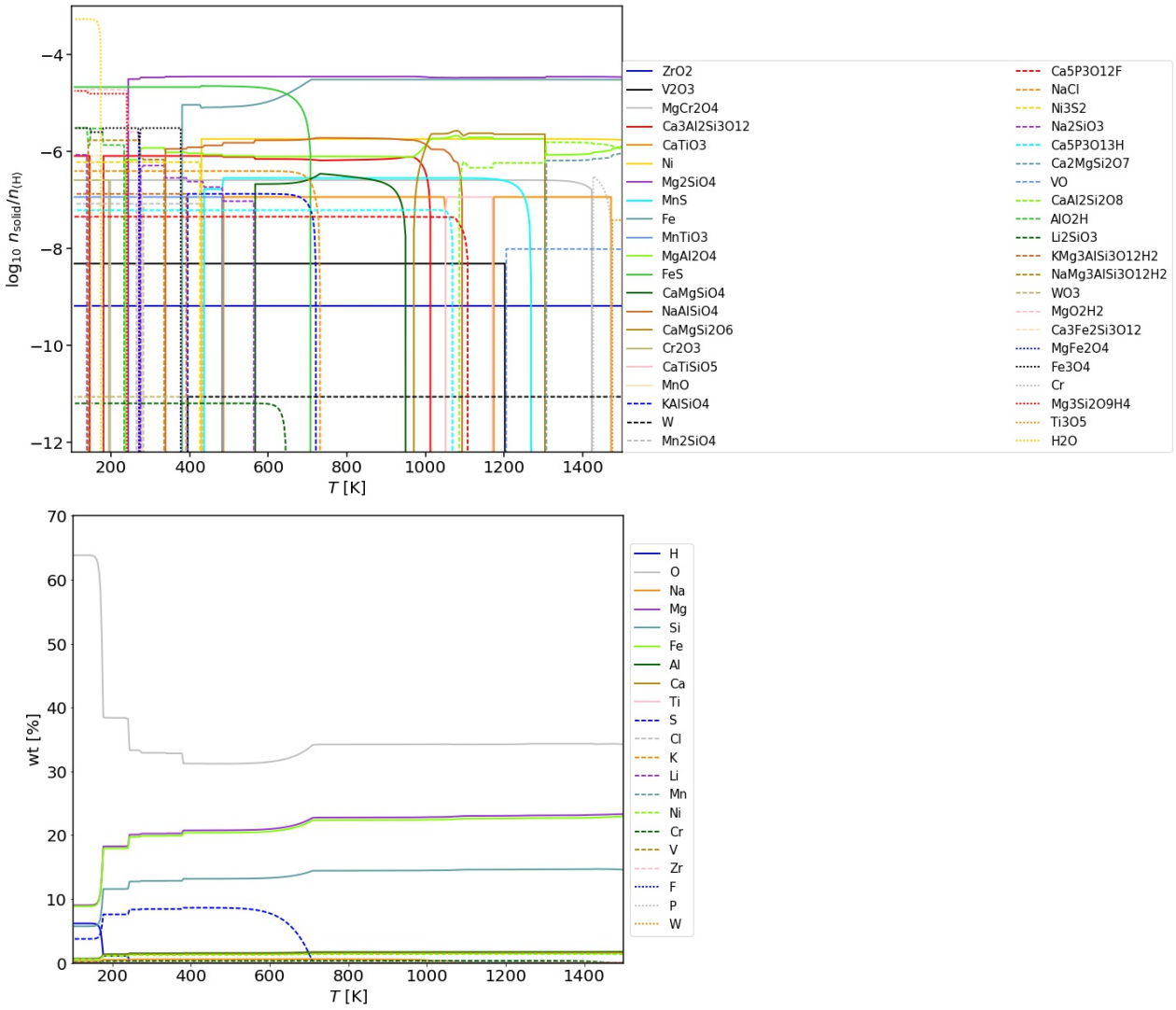

Figure 12: **Upper graph** Condensation sequence for HIP 63048 (star 3). The star is located on the right side of the graph. Smooth condensation (round edge) represent phase transition gas/solid, while sharp condensation represents phase transition solid/solid.
Lower graph The condensation sequence is translated into a graph showing the mass fraction of each element as a percentage.

B.5 HIP 43393

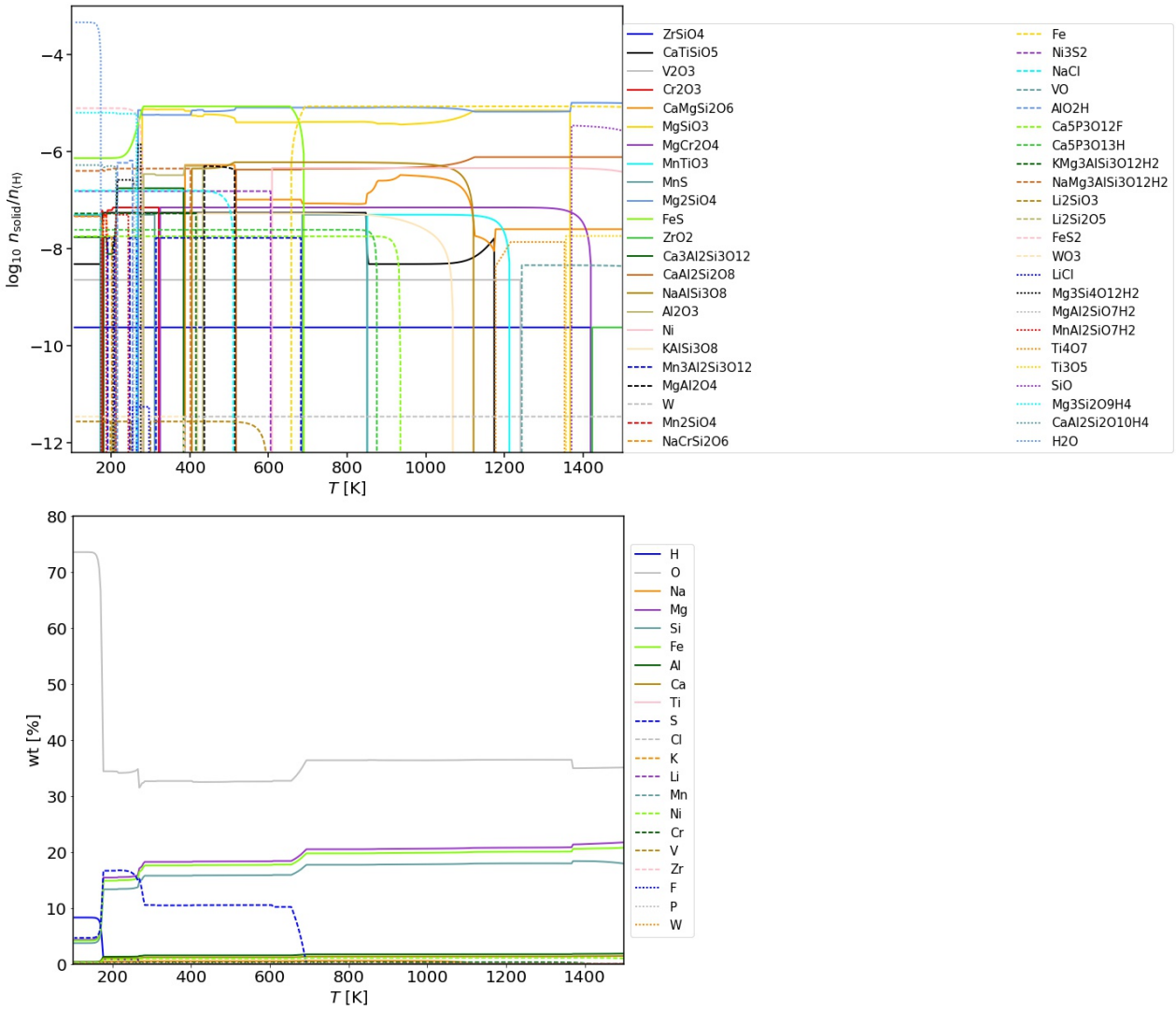

Figure 13: **Upper graph** Condensation sequence for HIP 43393 (star 4). The star is located on the right side of the graph. Smooth condensation (round edge) represent phase transition gas/solid, while sharp condensation represents phase transition solid/solid.
Lower graph The condensation sequence is translated into a graph showing the mass fraction of each element as a percentage.

B.6 HIP 99423

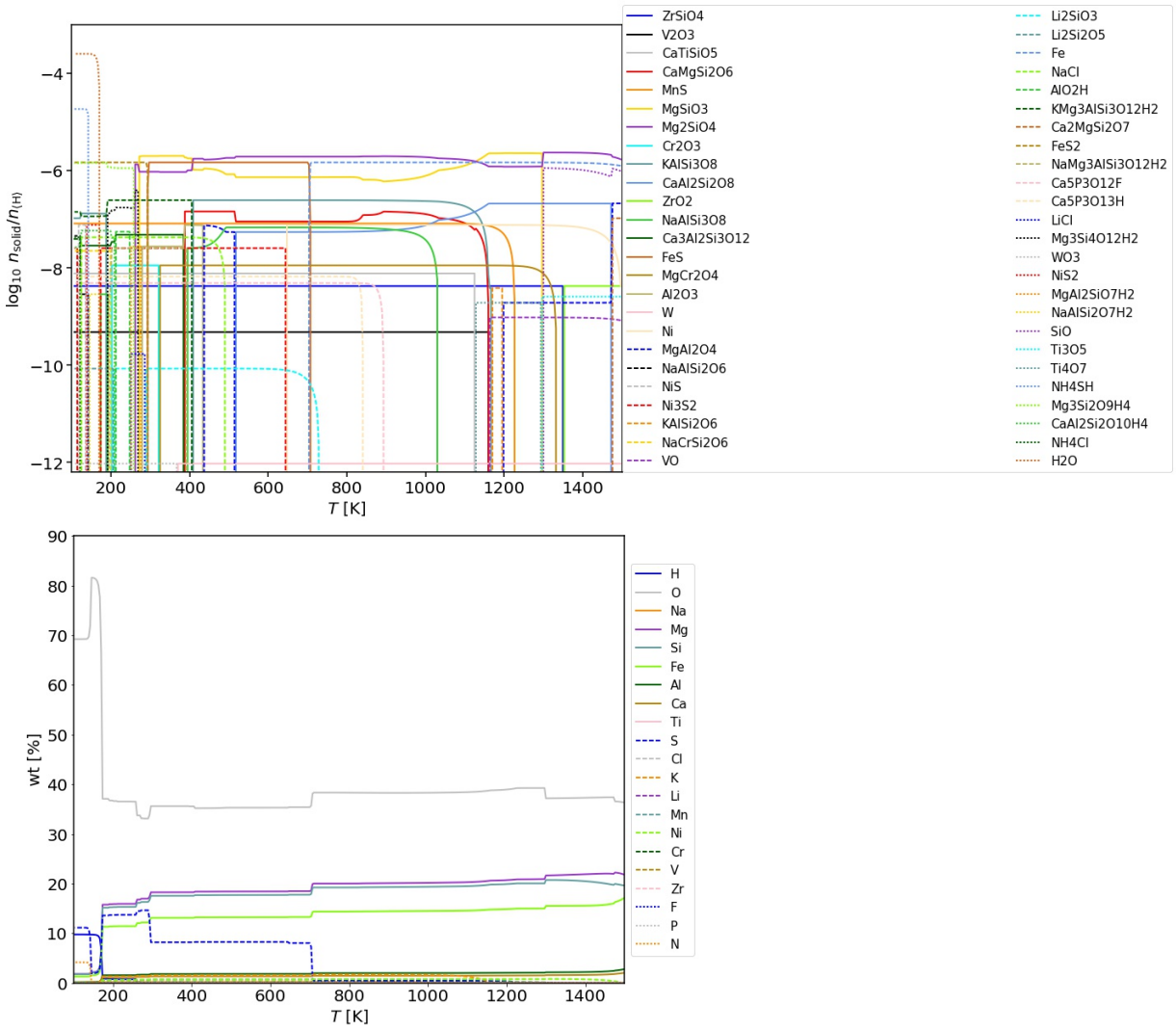

Figure 14: **Upper graph** Condensation sequence for HIP 99423 (star 5). The star is located on the right side of the graph. Smooth condensation (round edge) represent phase transition gas/solid, while sharp condensation represents phase transition solid/solid.
Lower graph The condensation sequence is translated into a graph showing the mass fraction of each element as a percentage.

B.7 HIP 83359

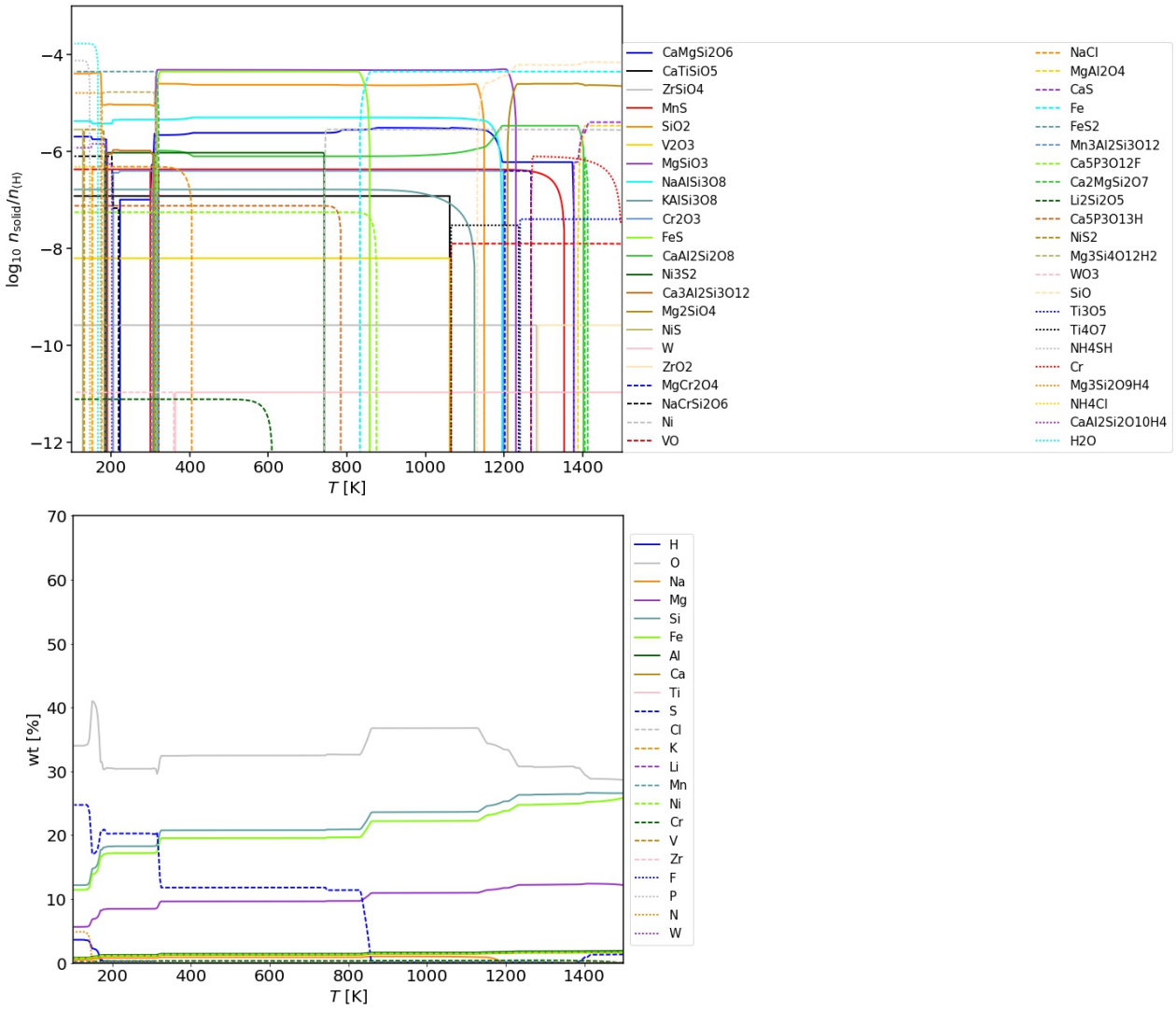

Figure 15: **Upper graph** Condensation sequence for HIP 83359 (star 6). The star is located on the right side of the graph. Smooth condensation (round edge) represent phase transition gas/solid, while sharp condensation represents phase transition solid/solid.
Lower graph The condensation sequence is translated into a graph showing the mass fraction of each element as a percentage.

C Mass fraction

Planet	'Mercury' (0.39 AU)							'Venus' (0.72 AU)						
Star	0	1	2	3	4	5	6	0	1	2	3	4	5	6
O	32.00	30.64	32.33	31.22	32.70	35.57	32.47	36.81	34.22	34.36	33.31	34.43	36.52	30.40
Mg	14.84	10.55	9.66	20.76	18.26	18.28	9.66	13.65	9.96	9.33	20.10	15.65	15.95	8.50
Si	13.94	13.53	16.50	13.18	15.78	17.57	20.79	12.82	12.76	15.95	12.76	13.53	15.33	18.29
Fe	27.09	33.47	29.25	20.39	17.61	13.13	19.56	24.90	31.58	28.26	19.74	15.09	11.46	17.21
S	6.48	6.18	6.84	8.66	10.47	8.22	11.82	5.96	5.83	6.61	8.38	16.05	13.75	20.27
Planet	'Earth' (1 AU)							'Mars' (1.52 AU)						
Star	0	1	2	3	4	5	6	0	1	2	3	4	5	6
O	37.14	35.52	36.58	38.37	34.43	36.74	30.49	60.35	57.69	56.84	63.80	73.57	81.59	38.10
Mg	13.55	9.70	8.93	18.26	15.43	15.88	8.49	7.47	5.66	5.46	9.06	4.33	2.19	6.36
Si	12.73	12.43	15.26	11.60	13.34	15.27	18.26	7.01	7.26	9.33	5.75	3.74	2.10	13.68
Fe	24.74	30.76	27.04	17.94	14.89	11.41	17.18	13.63	17.97	16.53	8.90	4.17	1.57	12.87
S	5.92	5.68	6.33	7.62	16.67	13.69	20.24	3.26	3.32	3.87	3.78	4.67	1.95	20.33
Planet	'Asteroid' (2.48 AU)													
Star	0	1	2	3	4	5	6							
O	60.39	57.71	56.88	63.82	73.59	69.22	34.01							
Mg	7.46	5.66	5.45	9.05	4.32	1.85	5.67							
Si	7.00	7.26	9.32	5.75	3.73	1.78	12.19							
Fe	13.61	17.95	16.51	8.89	4.17	1.33	11.47							
S	3.26	3.31	3.86	3.77	4.66	11.15	24.75							

Table 3: Mass fraction of five bodies forming *in situ* at the respective distance of Mercury, Venus, Earth, Mars and the Asteroid belt in the Solar system. Values are given as percentage of the total mass of the body [wt %].

D Chemical elements ratios (condensed phase)

Star	0	1	2	3	4	5	6
Fe/O	+0.000	+0.140	+0.110	-0.209	-0.600	-1.070	+0.175
Mg/O	+0.000	-0.100	-0.110	+0.060	-0.323	-0.665	+0.130
Si/O	+0.000	+0.035	+0.150	-0.11	-0.359	-0.655	+0.490
Fe/Si	+0.000	+0.105	-0.04	-0.099	-0.241	-0.415	-0.315
Mg/Si	+0.000	-0.135	-0.260	+0.170	+0.036	-0.010	-0.360
Fe/S	+0.000	+0.113	+0.010	-0.249	-0.670	-1.545	-0.955

Planet	'Mercury' (0.39 AU)							'Venus' (0.72 AU)						
Star	0	1	2	3	4	5	6	0	1	2	3	4	5	6
Si/O	+0.575	+0.580	+0.644	+0.562	+0.620	+0.629	+0.743	+0.477	+0.507	+0.602	+0.519	+0.531	+0.559	+0.716
Fe/O	+0.573	+0.683	+0.600	+0.459	+0.375	+0.212	+0.425	+0.475	+0.609	+0.560	+0.418	+0.287	+0.141	+0.397
Mg/O	+0.576	+0.448	+0.386	+0.733	+0.657	+0.620	+0.384	+0.479	+0.375	+0.344	+0.690	+0.567	+0.549	+0.356
Fe/Si	+0.000	+0.105	-0.040	-0.099	-0.241	-0.415	-0.315	+0.000	+0.105	-0.040	-0.099	-0.241	-0.415	-0.315
Mg/Si	+0.000	-0.135	-0.260	+0.170	+0.036	-0.010	-0.360	+0.000	-0.135	-0.260	+0.170	+0.036	-0.010	-0.360
Fe/S	+0.000	+0.113	+0.010	-0.249	-0.396	-0.418	-0.402	+0.000	+0.113	+0.010	-0.249	-0.648	-0.701	-0.693

Planet	'Earth' (1 AU)							'Mars' (1.52 AU)						
Star	0	1	2	3	4	5	6	0	1	2	3	4	5	6
Si/O	+0.470	+0.479	+0.557	+0.416	+0.525	+0.555	+0.713	+0.000	+0.04	+0.154	-0.112	-0.357	-0.643	+0.492
Fe/O	+0.468	+0.582	+0.513	+0.314	+0.281	+0.136	+0.394	+0.000	+0.136	+0.106	-0.211	-0.609	-1.035	+0.174
Mg/O	+0.472	+0.347	+0.298	+0.587	+0.561	+0.546	+0.354	+0.000	-0.096	-0.109	+0.060	-0.317	-0.653	+0.133
Fe/Si	+0.000	+0.105	-0.040	-0.099	-0.241	-0.415	-0.315	+0.000	+0.105	-0.040	-0.099	-0.241	-0.415	-0.315
Mg/Si	+0.000	-0.135	-0.260	+0.170	+0.036	-0.010	-0.360	+0.000	-0.135	-0.260	+0.170	+0.036	-0.010	-0.360
Fe/S	+0.000	+0.113	+0.010	-0.249	-0.670	-0.701	-0.693	+0.000	+0.113	+0.010	-0.249	-0.670	-0.71	-0.819

Planet	'Asteroid' (2.48 AU)						
Star	0	1	2	3	4	5	6
Si/O	+0.000	+0.04	+0.149	-0.112	-0.357	-0.643	+0.490
Fe/O	+0.000	+0.136	+0.106	-0.211	-0.609	-1.114	+0.174
Mg/O	+0.000	-0.096	-0.109	+0.060	-0.317	-0.653	+0.133
Fe/Si	+0.000	+0.105	-0.040	-0.099	-0.241	-0.415	-0.315
Mg/Si	+0.000	-0.135	-0.260	+0.170	+0.036	-0.010	-0.360
Fe/S	+0.000	+0.113	+0.010	-0.249	-0.670	-1.55	-0.955

Table 4: Chemical elements ratios found in the condensed phase from which 5 fictitious planets forming *in situ* at the respective distances of Mercury, Venus, Earth, Mars and Asteroid in the Solar System. Ratios are normalised by the Solar value (Eq 3). The upper most table represents the values of these ratios found in the gas phase before condensation. The subsequent tables, labelled with the names of the planets represent the values of these ratios in the condensed phase from which they form.

References

Armitage, P. (2019). *Chapter 1: Physical processes in protoplanetary disks*. Berlin,Heidelberg, Springer.

Asplund, M., Grevesse, N., Sauval, J., & Scott, P. (2009). The chemical composition of the sun. *Annual Review of Astronomy Astrophysics*, *47*(1). https://doi.org/10.1146/annurev.astro.46.060407.145222

Birch, F. (1952). Elasticity and constitution of the earth's interior. *Journal of Geophysical Research*, *57*(2). https://doi.org/10.1029/JZ057i002p00227

Blecic, J., Harrington, J., & Bowman, M. (2016). Tea: A code calculating thermochemical equilibrium abundances. *The Astrophysical Journal Supplement Series*, *225*(1). https://doi.org/10.3847/0067-0049/225/1/4

Boss, A. (1997). Giant planet formation by gravitational instability. *Science*, *276*. https://doi.org/10.1126/science.276.5320.1836

Chase, M., Curnutt, J., & Downey, J. (1982). Janaf thermochemical tables. *Journal of Physical and Chemical Reference Daa Monographs or Supplements*, *11*.

D'Alessio, P., Cantö, J., Calvet, N., & Lizano, S. (1998). Accretion disks around young objects. i. the detailed vertical structure. *The Astrophysical Journal*, *500*(1). https://doi.org/10.1086/305702

Dorn, C., Hinkel, N., & Venturini, J. (2017). Bayesian analysis of interiors of hd 219134b, kepler-10b, kepler-93b, corot-7b, 55 cnc e, and hd 97658b using stellar abundance proxies. *Astronomy Astrophysics*, *97*(A38). https://doi.org/10.1051/0004-6361/201628749

Gail, H., & Sedlmayr, E. (1986). The primary condensation process for dust around late m-type stars. *Astronomy Astrophysics*, *166*.

Hayashi, C. (1981). *Formation of the planets*. Dordrecht, D. Reidel Publishing Co.

Hinkel, N., Timmes, F., Young, P., Pagano, M., & Turnbull, M. (2014). Stellar abundances in the solar neighborhood: The hypatia catalog. *The Astronomical Journal*, *148*(3). https://doi.org/10.1088/0004-6256/148/3/54

Hinkel, N., Young, P., Pagano, M., & Turnbull, M. (2016). A comparison of stellar elemental abundance techniques and measurements. *The Astronomical Journal Supplement Series*, *226*(1). https://doi.org/10.3847/0067-0049/226/1/4

Hirose, K., Labrosse, S., & Hernlund, J. (2013). Composition and state of the core. *Annual Review of Earth and Planetary Sciences*, *41*. https://doi.org/10.1146/annurev-earth-050212-124007

Johnson, J., Oelkers, E., & Helgeson, H. (1992). Supcrt92: A software package for calculating the standard molal thermodynamic properties of minerals, gases, aqueous species, and reactions from 1 to 5000 bar and 0 to 1000c. *Computers and Geosciences*, *18*(7). https://doi.org/10.1016/0098-3004(92)90029-Q

Jr, M. C. (1986). Janaf thermochemical tables.

Kobayashi, H., Kimura, H., Watanabe, S., Yamamoto, T., & Müller, S. (2011). Sublimation temperature of circumstellar dust particles and its importance for dust ring formation. *Earth, Planet and Space*, *63*(6). https://doi.org/10.5047/eps.2011.03.012

Kobayashi, H., Watanabe, S., Kimura, H., & Yamamoto, T. (2009). Dust ring formation due to sublimation of dust grains drifting radially inward by the poynting-robertson drag: An analytical model. *Icarus*, *201*(1). https://doi.org/10.1016/j.icarus.2009.01.002

Kobayashi, & Nakasato, N. (2011). Chemodynamical simulations of the milky way galaxy. *The Astrophysical Journal*, *729*(1). https://doi.org/10.1088/0004-637X/729/1/16

Liu, Y., Sato, B., Takeda, Y., Ando, H., & Zhao, G. (2010). Stellar parameters and abundance analysis of 58 late g giants. *Publications of the Astronomical Society of Japan*, *62*(4). https://doi.org/10.1093/pasj/62.4.1071

Pollack, J., Hubickyj, O., Bodenheimer, P., Lissauer, J., Podolak, M., & Greenzweig, Y. (1996). Formation of the giant planets by concurrent accretion of solids and gas. *Icarus*, *124*(1). https://doi.org/10.1006/icar.1996.0190

Thiabaud, A., Marboeuf, U., Alibert, Y., Leya, I., & Mezger, K. (2015). Elemental ratios in stas vs planets. *Astronomy Astrophysics*, *580*(A30). https://doi.org/10.1051/0004-6361/201525963

Tuthill, P., Monnier, J., & Danchi, W. (2001). A dusty torus around the luminous young star lkhα101. *Nature*, *409*. https://doi.org/10.1038/35059014

Unterborn, C., Dismukes, E., & Panero, W. (2016). Scaling the earth: A sensitivity analysis of terrestrial exoplanetary interior models. *The Astrophysical Journal*, *819*(1). https://doi.org/10.3847/0004-637X/819/1/32

Woitke, P., Helling, C., Hunter, G., Millard, J., Turner, G., Worters, M., Blecic, J., & Stock, J. (2018). Equilibrium chemistry down to 100 k. impact of silicates and phyllosilicates on the carbon to oxygen ratio. *Astronomy Astrophysics*, *614*(A1). https://doi.org/10.1051/0004-6361/201732193

Zimmer, K., Zhang, Y., Lu, P., Chen, Y., Zhang, G., Dalkilic, M., & Zhu, C. (2016). Supcrtbl: A revised and extended thermodynamic dataset and software package of supcrt92. *Computers and Geosciences*, *90*. https://doi.org/10.1016/j.cageo.2016.02.013